





RESEARCH ARTICLE

WILEY

Cardiometabolic risk factors associated with brain age and accelerate brain ageing

Dani Beck^{1,2,3}  | Ann-Marie G. de Lange^{1,4,5} | Mads L. Pedersen^{1,2} |
 Dag Alnæs^{1,6} | Ivan I. Maximov^{1,2,7} | Irene Voldsbekk^{1,2}  |
 Geneviève Richard¹  | Anne-Marthe Sanders^{1,2,3} | Kristine M. Ulrichsen^{1,2,3} |
 Erlend S. Dørum^{1,2,3} | Knut K. Kolskår^{1,2,3} | Einar A. Høgestøl^{1,2} | Nils Eiel Steen¹ |
 Srdjan Djurovic¹ | Ole A. Andreassen^{1,8} | Jan E. Nordvik⁹ | Tobias Kaufmann^{1,10} |
 Lars T. Westlye^{1,2,8} 

¹NORMENT, Division of Mental Health and Addiction, Oslo University Hospital & Institute of Clinical Medicine, University of Oslo, Oslo

²Department of Psychology, University of Oslo, Oslo

³Sunnaas Rehabilitation Hospital HT, Nesodden

⁴LREN, Centre for Research in Neurosciences-Department of Clinical Neurosciences, CHUV and University of Lausanne, Lausanne, Switzerland

⁵Department of Psychiatry, University of Oxford, Oxford, UK

⁶Bjørknes College, Oslo, Norway

⁷Department of Health and Functioning, Western Norway University of Applied Sciences, Bergen, Norway

⁸KG Jebsen Centre for Neurodevelopmental Disorders, University of Oslo, Oslo, Norway

⁹CatoSenteret Rehabilitation Center, Son, Norway

¹⁰Department of Psychiatry and Psychotherapy, University of Tübingen, Tübingen, Germany

Correspondence

Dani Beck and Lars T. Westlye, Department of Psychology, University of Oslo, PO Box 1094 Blindern, Oslo 0317, Norway.

Email: dani.beck@psykologi.uio.no (D. B.) and l.t.westlye@psykologi.uio.no (L. T. W)

Funding information

EkstraStiftelsen Helse og Rehabilitering, Grant/Award Number: 2015/FO5146; German Federal Ministry of Education and Research, Grant/Award Number: 01ZX1904A; H2020 European Research Council, Grant/Award Numbers: 802998, 847776; Helse Sør-Øst RHF, Grant/Award Numbers: 2014097, 2015044, 2015073, 2016083, 2018037, 2018076; Norges Forskningsråd, Grant/Award Numbers: 223273, 248238, 249795, 276082, 298646; Stiftelsen Kristian Gerhard Jebsen, Grant/Award Number: PZ00P3_193658

Abstract

The structure and integrity of the ageing brain is interchangeably linked to physical health, and cardiometabolic risk factors (CMRs) are associated with dementia and other brain disorders. In this mixed cross-sectional and longitudinal study (interval mean = 19.7 months), including 790 healthy individuals (mean age = 46.7 years, 53% women), we investigated CMRs and health indicators including anthropometric measures, lifestyle factors, and blood biomarkers in relation to brain structure using MRI-based morphometry and diffusion tensor imaging (DTI). We performed tissue specific brain age prediction using machine learning and performed Bayesian multilevel modeling to assess changes in each CMR over time, their respective association with brain age gap (BAG), and their interaction effects with time and age on the tissue-specific BAGs. The results showed credible associations between DTI-based BAG and blood levels of phosphate and mean cell volume (MCV), and between T1-based BAG and systolic blood pressure, smoking, pulse, and C-reactive protein (CRP), indicating older-appearing brains in people with higher cardiometabolic risk (smoking, higher blood pressure and pulse, low-grade

This is an open access article under the terms of the Creative Commons Attribution-NonCommercial-NoDerivs License, which permits use and distribution in any medium, provided the original work is properly cited, the use is non-commercial and no modifications or adaptations are made.

© 2021 The Authors. *Human Brain Mapping* published by Wiley Periodicals LLC.

inflammation). Longitudinal evidence supported interactions between both BAGs and waist-to-hip ratio (WHR), and between DTI-based BAG and systolic blood pressure and smoking, indicating accelerated ageing in people with higher cardiometabolic risk (smoking, higher blood pressure, and WHR). The results demonstrate that cardiometabolic risk factors are associated with brain ageing. While randomized controlled trials are needed to establish causality, our results indicate that public health initiatives and treatment strategies targeting modifiable cardiometabolic risk factors may also improve risk trajectories and delay brain ageing.

KEYWORDS

brain age, cardiometabolic risk, DTI, T1 MRI

1 | INTRODUCTION

It is well established that various cardiometabolic risk factors (CMRs) are associated with an increased risk of a range of brain disorders, including stroke, Alzheimer's disease and other dementias, in addition to ageing-related cognitive decline, supporting an intimate body-brain connection in ageing (Qiu & Fratiglioni, 2015). Moreover, associations between high insulin and obesity in childhood and risk for psychosis and depression at 24 years of age indicate that CMRs in childhood represent predictors for mental disorders later in life (Perry et al., 2021). Research has found that established CMRs such as blood pressure (Fuhrmann et al., 2019; Verhaaren et al., 2013), WHR, body mass index (BMI) (Karlsson et al., 2013; Spangaro, Mazza, Poletti, Cavallaro, & Benedetti, 2018), diabetes mellitus (Hooogenboom et al., 2014; Hsu et al., 2012), hypertension (McEvoy et al., 2015), total elevated cholesterol (Walhovd, Storsve, Westlye, Drevon, & Fjell, 2014; Williams et al., 2018), smoking (Jeerakathil et al., 2004), and high low-density lipoprotein (LDL) cholesterol (Murray et al., 2005), are all associated with brain structure to various degrees. However, there is substantial variability among individuals in terms of impact on the brain and the putative biological factors involved.

Brain-predicted age has recently emerged as a reliable and heritable biomarker of brain health and ageing (Cole et al., 2017; Franke, Ziegler, Klöppel, & Gaser, 2010; Kaufmann et al., 2019). The difference between the brain-predicted age and chronological age—also referred to as the brain age gap (BAG)—can be used to assess deviations from expected age trajectories. These estimations of brain age may thus have clinical implications, as identifying factors associated with higher BAG and accelerated ageing can help us detect potential targets for intervention strategies.

Higher brain age has been associated with poorer cognitive functioning in healthy individuals (Richard et al., 2018) and people with cognitive impairment (Varatharajah et al., 2018), mild cognitive impairment (MCI), dementia (Kaufmann et al., 2019), and mortality in elderly people (Cole et al., 2018). Larger BAGs have also been reported among patients with psychiatric and neurological disorders, including schizophrenia, bipolar disorder, multiple sclerosis (Høgestøl et al., 2019; Kaufmann et al., 2019; Tønnesen et al., 2020), depression (Han et al., 2020), and epilepsy (Pardoe, Cole, Blackmon, Thesen, & Kuzniecky, 2017; Sone et al., 2019).

While BAG shows substantial heritability (Cole et al., 2017; Kaufmann et al., 2019), the rate of brain ageing is malleable and dependent on a range of life events and health and lifestyle factors (Cole, 2020; Lindenberger, 2014; Sanders et al., 2021). Understanding the impact of cardiometabolic risk on brain integrity and ageing represents a window of opportunity wherein interventions targeting key elements of cardiometabolic health may delay and even prevent pathological brain changes (Friedman et al., 2014).

Studies assessing cardiometabolic risk have reported brain age associations with diastolic blood pressure, BMI (Franke, Ristow, & Gaser, 2014), obesity (Kolenic et al., 2018; Ronan et al., 2016), and diabetes (Franke, Gaser, Manor, & Novak, 2013). Larger BAGs have also been associated with high blood pressure, alcohol intake, diabetes, smoking, and history of stroke in the UK Biobank (Cole, 2020), and with high blood pressure, alcohol intake, and stroke risk scores in the Whitehall II MRI sub-sample (de Lange et al., 2020). Despite existing research, the links between cardiometabolic risk and brain ageing are still unclear. Longitudinal studies utilizing multimodal imaging may aid to link individual CMRs to tissue specific effects.

By including cross-sectional and longitudinal data obtained from 790 healthy subjects aged 18–94 years (mean 46.7, *SD* 16.3), our primary aim was to investigate how key CMRs interact with tissue-specific (DTI and T1-weighted) measures of brain ageing. We investigated longitudinal associations between brain age and a range of CMRs and tested both for main effects across time and interactions with age and time. Adopting a Bayesian statistical framework, we hypothesized that key indicators of cardiometabolic risk would be associated with more apparent brain ageing, both reflected as main effects across time, and as interactions, indicating a faster pace of brain ageing over the course of the follow-up period in people with high cardiometabolic risk.

2 | MATERIAL AND METHODS

2.1 | Sample description

The initial sample consisted of 1,130 (832 baseline, 298 follow up) datasets from 832 healthy participants from two integrated studies;

TABLE 1 Sample descriptives at baseline and follow-up

	Baseline sample (n = 790)	Follow-up sample (n = 272)
Age (mean ± SD)	46.7 ± 16.3	57.8 ± 15.0
Sex (%)		
Male	372 (47.09%)	106 (38.97%)
Female	418 (52.91%)	166 (61.03%)

the Thematically Organized Psychosis (TOP) (Tønnesen et al., 2018) and StrokeMRI (Richard et al., 2018). Exclusion criteria included neurological and mental disorders, and previous head trauma. The study was conducted in line with the Declaration of Helsinki and approved by the Regional Ethics Committee, and all participants provided written informed consent. The data and code used in the study is freely available in a public repository—Open Science Framework (OSF)—and accessible directly through the OSF webpage (<https://osf.io/ujwat/>).

Following the removal of 68 MRI datasets after quality checking (QC) of the MRI data (see Section 2.5), the final sample comprised 1,062 datasets from 790 individuals, including longitudinal data (two time-points with 19.7 months interval on average (min = 9.8, max = 35.6) from 272 participants. Demographic information of the test sample is summarized in Table 1, Figure 1.

Data from the Cambridge Centre for Ageing and Neuroscience (Cam-CAN; <http://www.mrc-cbu.cam.ac.uk/datasets/camcan/>; Shafto et al., 2014; Taylor et al., 2017) was used as an independent training sample for brain age prediction (see Section 2.6). After QC, MRI data from 622 participants were included (age range = 18–87, mean age ± standard deviation = 54.2 ± 18.4). Figure S1 shows the age distribution for the training and test samples.

2.2 | MRI acquisition

MRI was performed at Oslo University Hospital on a GE Discovery MR750 3T scanner with a 32-channel head coil. DTI data were acquired with a spin echo planar imaging (EPI) sequence with the following parameters: repetition time (TR)/echo time (TE)/flip angle: 8,150 ms/83.1 ms/90°, FOV: 256 × 256 mm², slice thickness: 2 mm, in-plane resolution: 2 × 2 mm², 60 noncoplanar directions ($b = 1,000$ s/mm²), and 5 $b = 0$ volumes, scan time: 8:58 min. In addition, 7 $b = 0$ volumes with reversed phase-encoding direction were acquired. High-resolution T1-weighted data was acquired using a 3D inversion recovery prepared fast spoiled gradient recalled sequence (IR-FSPGR; BRAVO) with the following parameters: TR: 8.16 ms, TE: 3.18 ms, flip angle: 12°, voxel size: 1 × 1 × 1 mm³, FOV: 256 × 256 mm², 188 sagittal slices, scan time: 4:43 min.

For the Cam-CAN training set, participants were scanned on a 3T Siemens TIM Trio scanner with a 32-channel head-coil at Medical Research Council (UK) Cognition and Brain Sciences Unit (MRC-CBSU) in Cambridge, UK. DTI data was acquired using a twice—refocused spin echo sequence with the following parameters a TR: 9,100 ms, TE: 104 ms, FOV: 192 × 192 mm², voxel size: 2 mm,

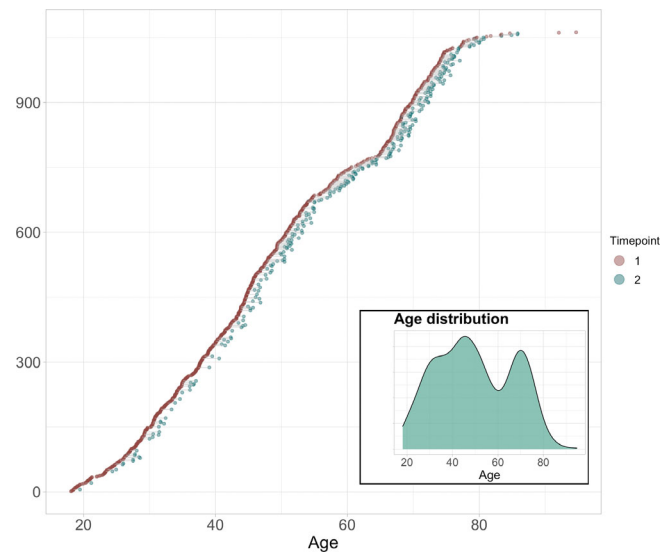


FIGURE 1 Available baseline and follow-up data. All participants are shown. Participants with data at baseline are visualized in red dots ($N = 790$). The subset ($n = 272$) with longitudinal measures are connected to corresponding timepoint with green dots. The mean interval between timepoints was 1.64 years ($SD = 0.5$ years). Subplot shows age distribution at baseline

66 axial slices using 30 directions with $b = 1,000$ s/mm², 30 directions with $b = 2,000$ s/mm², and 3 $b = 0$ images (Shafto et al., 2014). High-resolution 3D T1-weighted data were acquired using a magnetization prepared rapid gradient echo (MPRAGE) sequence with the following parameters: TR: 2,250 ms, TE: 2.99 ms, inversion time (TI): 900 ms, flip angle: 9°, FOV of 256 × 240 × 192 mm³; voxel size = 1 × 1 × 1 mm³, GRAPPA acceleration factor of 2, scan time 4:32 min (Shafto et al., 2014).

2.3 | DTI processing and TBSS analysis

Processing steps for single-shell DTI data in the test set followed a previously described pipeline (Maximov, Alnæs, & Westlye, 2019), including noise correction (Veraart, Fieremans, & Novikov, 2016), Gibbs ringing correction (Kellner, Dhital, Kiselev, & Reisert, 2016), corrections for susceptibility induced distortions, head movements and eddy current induced distortions using topup (<http://fsl.fmrib.ox.ac.uk/fsl/fslwiki/topup>) and eddy (<http://fsl.fmrib.ox.ac.uk/fsl/fslwiki/eddy>; Andersson & Sotiropoulos, 2016). Isotropic smoothing was carried out with a Gaussian kernel of 1 mm³ implemented in the FSL function *fslmaths*. DTI metrics were estimated using *dtifit* in FSL and a weighted least squares algorithm. Processing steps for the training set followed a similar pipeline with the exception of the noise correction procedure. Voxelwise statistical analysis of the fractional anisotropy (FA) data was carried out using Tract-Based Spatial Statistics (TBSS) (Smith et al., 2006), as part of FSL (Smith et al., 2004). First, FA images were brain-extracted using BET (Smith, 2002) and aligned into a common space (FMR158_FA template) using the nonlinear registration tool FNIRT (Jenkinson, Beckmann, Behrens, Woolrich, & Smith, 2012),

which uses a b-spline representation of the registration warp field (Rueckert et al., 1999). Next, the mean FA image of all subjects was created and thinned to create a mean FA skeleton that represents the centers of all tracts common to the group. Each subject's aligned FA data was then projected onto this skeleton. The mean FA skeleton was thresholded at $FA > 0.2$. This procedure was repeated in order to extract axial diffusivity (AD), mean diffusivity (MD), and radial diffusivity (RD). *fslmeants* was used to extract the mean skeleton and 20 regions of interest (ROIs) based on a probabilistic white matter atlas (JHU) (Hua et al., 2008) for each metric. Including the mean skeleton values, 276 features per individual were derived in total.

2.4 | FreeSurfer processing

T1-weighted MRI data were processed using FreeSurfer (Fischl, 2012) 7.1.0 for the test set and FreeSurfer 5.3 for the training set. To extract reliable area, volume, and thickness estimates, the test set including follow-up data were processed with the longitudinal stream (Reuter, Schmansky, Rosas, & Fischl, 2012) in FreeSurfer. Specifically, an unbiased within-subject template space and image (Reuter & Fischl, 2011) is created using robust, inverse consistent registration (Reuter, Rosas, & Fischl, 2010). Several processing steps, such as skull stripping, Talairach transforms, atlas registration as well as spherical surface maps and parcellations are then initialized with common information from the within-subject template, significantly increasing reliability and statistical power (Reuter et al., 2012). Due to the longitudinal stream in FreeSurfer influencing the thickness estimates, and subsequently having an impact on brain age prediction (Høgestøl et al., 2019), both cross-sectional and longitudinal data in the test set were processed with the longitudinal stream. Cortical parcellation was performed using the Desikan–Killiany atlas (Desikan et al., 2006), and subcortical segmentation was performed using a probabilistic atlas (Fischl et al., 2002). Two hundred sixty-nine FreeSurfer based features were extracted in total, including global features for intracranial volume, total surface area, and whole cortex mean thickness, as well as the volume of subcortical structures.

2.5 | QC procedure

Prior to statistical analyses, a rigorous QC procedure was implemented to ensure sufficient data quality.

For DTI data ($N = 1,130$) we derived various QC metrics (see Table S1), including temporal signal-to-noise-ratio (tSNR; Roalf et al., 2016). Datasets with tSNR $z > 2.5$ standard deviations from the mean were flagged and manually checked and removed if deemed to have unsatisfactory data quality. A total of 14 datasets were removed during QC, leaving the dataset at $n = 1,116$ scans.

For T1-weighted data, QC was carried out using the ENIGMA cortical QC protocol including three major steps: outlier detection, internal surface method, and external surface method. Quality ratings of each image were recorded using the ENIGMA cortical QC template

for each of the initial 1,130 dataset. A total of 16 datasets were removed, leaving the dataset at $n = 1,114$ scans. Next, the separate datasets from both T1 ($N = 1,114$) and DTI ($N = 1,116$) were merged to form a matching sample by subject ID, leaving the sample at $N = 1,101$, consisting of the same subjects that had quality checked data for both modalities. Finally, this sample was merged with the CMR data, leaving the final sample used for the study at $N = 1,062$.

2.6 | Brain age prediction

In line with previous studies (Kuhn et al., 2018; Richard et al., 2018), we used Cam-CAN to train the brain age prediction models. The model input included 276 features for the DTI-based age prediction and 269 features for the age prediction based on T1-weighted data, as described in Sections 2.3 and 2.4, and summarized in Table S2. Age prediction was performed using XGBoost regression (<https://xgboost.readthedocs.io/en/latest/python>), which is based on a decision-tree ensemble algorithm used in several recent brain age prediction studies (Beck et al., 2021; de Lange, Barth, et al., 2020; de Lange, Kaufmann, et al., 2019; de Lange et al., 2020; Kaufmann et al., 2019; Richard et al., 2020). Parameters were tuned in nested cross-validations using five inner folds for grid search (max depth: [2, 10, 1], number of estimators: [60, 220, 40], learning rate: [0.1, 0.01, 0.05]), and 10 outer folds for validating model performance within the training sample. The models were fitted using the best estimators, and the optimized models were applied to the test sample. R^2 , RMSE, and MAE were calculated to evaluate prediction accuracy in the test set. To adjust for a commonly observed age-bias (overestimated predictions for younger participants and underestimated predictions for older participants) (Liang, Zhang, & Niu, 2019), we applied a statistical correction as previously described in (de Lange & Cole, 2020); we first fitted $Y = \alpha \times \Omega + \beta$, where Y is the modeled predicted age as a function of chronological age (Ω), and α and β represent the slope and intercept. Next, we used the derived values of α and β to correct predicted age with *Corrected Predicted Age* = *Predicted Age* + $[\Omega - (\alpha \times \Omega + \beta)]$ before re-calculating R^2 , RMSE, and MAE. The age-bias correction procedure was performed in the test set, and is equivalent to removing the effect of chronological age from the predictions or BAG values (see e.g., Beheshti, Nugent, Potvin, & Duchesne, 2019; de Lange et al., 2021; Liang et al., 2019). BAG was calculated using (corrected predicted age—chronological age) for each of the models, providing T1 and DTI-based BAG values for all participants. To test if a nonlinear age-bias correction yielded different results, we corrected the predictions using a nonlinear correction (de Lange, Barth, et al., 2020; de Lange, Kaufmann, et al., 2019). These approaches showed highly comparable results, as shown in Figure S11.

2.7 | Cardiometabolic risk factors

Clinical information including BMI, systolic and diastolic blood pressure, pulse, WHR, and smoking were collected at the time of MRI,

with standard hospital biochemical blood measures being collected at a different site (Table S2). All participants underwent a physical examination. BMI (weight in kg/height in m²) was calculated from weighing the participants on calibrated digital weights wearing light clothing and no shoes. Waist circumference was measured midway between lowest rib and the iliac crest. Blood pressure was recorded in sitting position after resting before MRI scans were collected and after. Blood samples were drawn and analyzed for hemoglobin, erythrocyte indexes (MCV [mean corpuscular volume], MCH [mean corpuscular hemoglobin], MCHC [mean corpuscular hemoglobin concentration]), thrombocytes, sodium, potassium, chloride, calcium, magnesium, phosphate, creatinine, ALAT (alanine transaminase), CK (creatin kinase), LD (lactate dehydrogenase), GT (gamma-glutamyl transferase), CRP (C-reactive protein), total cholesterol, LDL (low-density lipoprotein) cholesterol, HDL (high-density lipoprotein) cholesterol, triglycerides, and glucose. Blood samples were analyzed at the Department of Medical Biochemistry, Oslo University Hospital, on several routine instruments: Integra 800, Abbot Architect, i2000, Cobas 8000 e602 and Cobas 8000 e801 (Roche Diagnostics, Basel, Switzerland: www.roche.com/about/business/diagnostics.html) using standard methods

controlled by internal and external quality control samples (Rødevand et al., 2019).

Missing entries (<15% for each variable) were imputed using the MICE package (van Buuren & Groothuis-Oudshoorn, 2011) in R, where five imputations were carried out using the predictive mean matching method (package default). The distribution of the original and imputed data was inspected (Figures S2–S5) and the imputed data were deemed as plausible values. Of the five imputations, the first was used for the remainder of the study. Additional QC was carried out on all CMRs using a multivariate outlier detection algorithm, where anomalies in the data are detected as observations that do not conform to an expected pattern to other items. Using the R package *mvoutlier* (Filzmoser, Garrett, & Reimann, 2005), potential outliers were flagged using the Mahalanobis distance (Figures S6 and S7). Informed by an interactive plot using the *chisq.plot* function, manual outlier observations of each of these flagged values deemed eight of them as true outliers (Figure S8), leading to their removal from the initial 1,120 CMR dataset, and leaving the dataset at 1,112. The final sample was further reduced to 1,062 datasets (from 790 individuals) when merged with the available MRI datasets ($N = 1,101$).

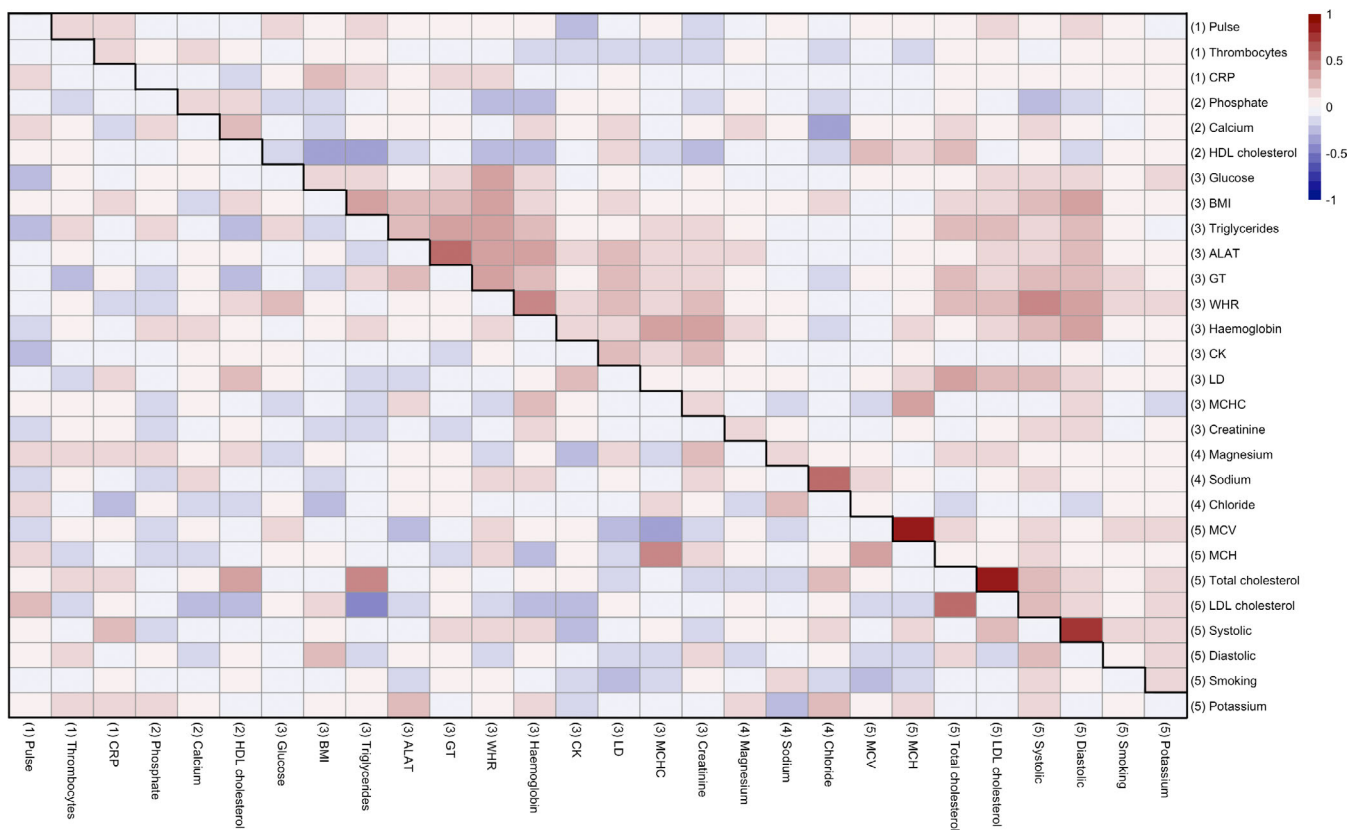


FIGURE 2 Associations between CMRs. Heatmap showing correlation matrix of all CMRs (scaled), where the lower diagonal shows partial correlations (calculated by taking the residuals from two associated resistant regression models and calculating the correlations between them), and the upper diagonal shows full correlations. Hierarchical clustering of the variables was performed based on the full correlations and revealed five cluster groups, shown by numbers in brackets. Table S3 provides a detailed overview of all abbreviations used and Figure S9 an overview of the hierarchical clustering-derived dendrogram used in the figure

To visualize the associations between the CMRs, hierarchical clustering of the variables was performed using “hclust,” part of the “stats” package in R (R Core Team, 2012), which uses the complete linkage method to form clusters. Five cluster groups were revealed. Figure 2 provides the full (upper diagonal) and partial (lower diagonal) correlations with results of hierarchical clustering represented by numbers in brackets for each variable.

2.8 | Statistical analysis

All statistical analyses were carried out using R, version 3.6.0 (www.r-project.org/; R Core Team, 2012). To investigate the associations between the CMRs and BAG, we carried out Bayesian multilevel models in “Stan” (Stan Development Team, 2019) using the *brms* (Bürkner, 2017, 2018) package in R (R Core Team, 2012). For descriptive purposes, we first tested associations between BAG and time. Here, BAG (for T1 and DTI separately) was entered as the dependent variable while timepoint was entered as the independent variable. Second, we tested associations between each CMR and time and age (chronological age calculated as years between date of birth and date of MRI scan). Here, timepoint and age were entered as the independent variable (in separate analyses). Third, to address the primary aim of the study, we tested for associations between BAG and each CMR across time. Here, BAG (for T1 and DTI separately) was entered as the dependent variable with each CMR separately entered as the independent fixed effects variable along with age, sex, and time, with subject ID as random effects. Fourth, in order to test our hypothesis that the associations between cardiometabolic risk and BAG vary as a function of age both cross-sectionally and longitudinally, interaction effects of CMR and age on BAG, and CMR and time on BAG, were included in the models as additional fixed effects. For each model, timepoint and age were included in the models where appropriate, while sex was added to every model. In order to prevent false positives and to regularize the estimated associations, we defined a strong normal prior around zero with a standard deviation of 0.3 for all coefficients bar BAG ~ time. For each coefficient of interest, we report the mean estimated value and its uncertainty measured by the 95% credible interval of the posterior

TABLE 2 Average R^2 , root mean square error (RMSE), and mean absolute error (MAE) \pm standard deviation for the age prediction models within the training sample (Cam-CAN), test set, and age-corrected test set

		Training sample (Cam-CAN)	Test set before age-bias correction	Test set after age-bias correction
DTI	R^2	.82 \pm .04	.72	.92
	RMSE	7.67 \pm 0.83	10.11	5.12
	MAE	6.15 \pm 0.55	8.37	4.06
T1	R^2	.81 \pm .04	.73	.87
	RMSE	RMSE	9.11	6.55
	MAE	MAE	7.2	5.21

distribution. We calculated Bayes factors (BFs) using the Savage-Dickey method (Wagenmakers, Lodewyckx, Kuriyal, & Grasman, 2010). For a pragmatic guide on BF interpretation, see Table S4.

TABLE 3 Descriptive statistics at baseline for each variable bar smoking, which is summarized in its own table due to its ordinal nature

	Mean \pm SD	Min	Max
Hematology			
Hemoglobin	14.2 \pm 1.2	9.8	18.6
MCHC	33.2 \pm 1	29	36
MCV	90.6 \pm 3.9	76	108
MCH	30 \pm 1.4	22.2	36.7
Thrombocytes	255.8 \pm 55.4	81	499
Electrolytes			
Phosphate	1.1 \pm 0.2	0.5	1.6
Calcium	2.4 \pm 0.1	2.1	2.9
Sodium	140.6 \pm 2.1	131	147
Chloride	101.6 \pm 2.2	93	107
Magnesium	0.9 \pm 0.1	0.6	1.1
Potassium	4.3 \pm 0.3	2.9	5.9
Metabolites			
Creatinine	74.7 \pm 13	46	115
Enzymes/Markers			
ALAT	24.7 \pm 12.3	3	97
CK	126.7 \pm 75	31	499
LD	168 \pm 29	83	293
GT	24.7 \pm 17.4	5	149
Carbohydrates			
Glucose	5.3 \pm 0.8	2.3	10.6
Proteins/Lipids			
HDL cholesterol	1.6 \pm 0.5	0.6	4.4
Total cholesterol	5.1 \pm 1.1	2.9	8.9
LDL cholesterol	3.2 \pm 0.9	1.2	6.4
CRP	1.6 \pm 1.7	0.4	12.2
Triglycerides	1.3 \pm 0.9	0.3	7.7
Clinical measures			
WHR	0.9 \pm 0.1	0.5	1.3
Systolic	127.6 \pm 17.5	90	190
Diastolic	80 \pm 9.6	50	113.7
Pulse	66 \pm 9.5	40	97.6
BMI	25.2 \pm 4.1	16.8	43.4

TABLE 4 Smoking at baseline

	Frequency (%)
Never smoked	593 (75.1)
Previous smoker	127 (16.0)
Current smoker	70 (8.9)

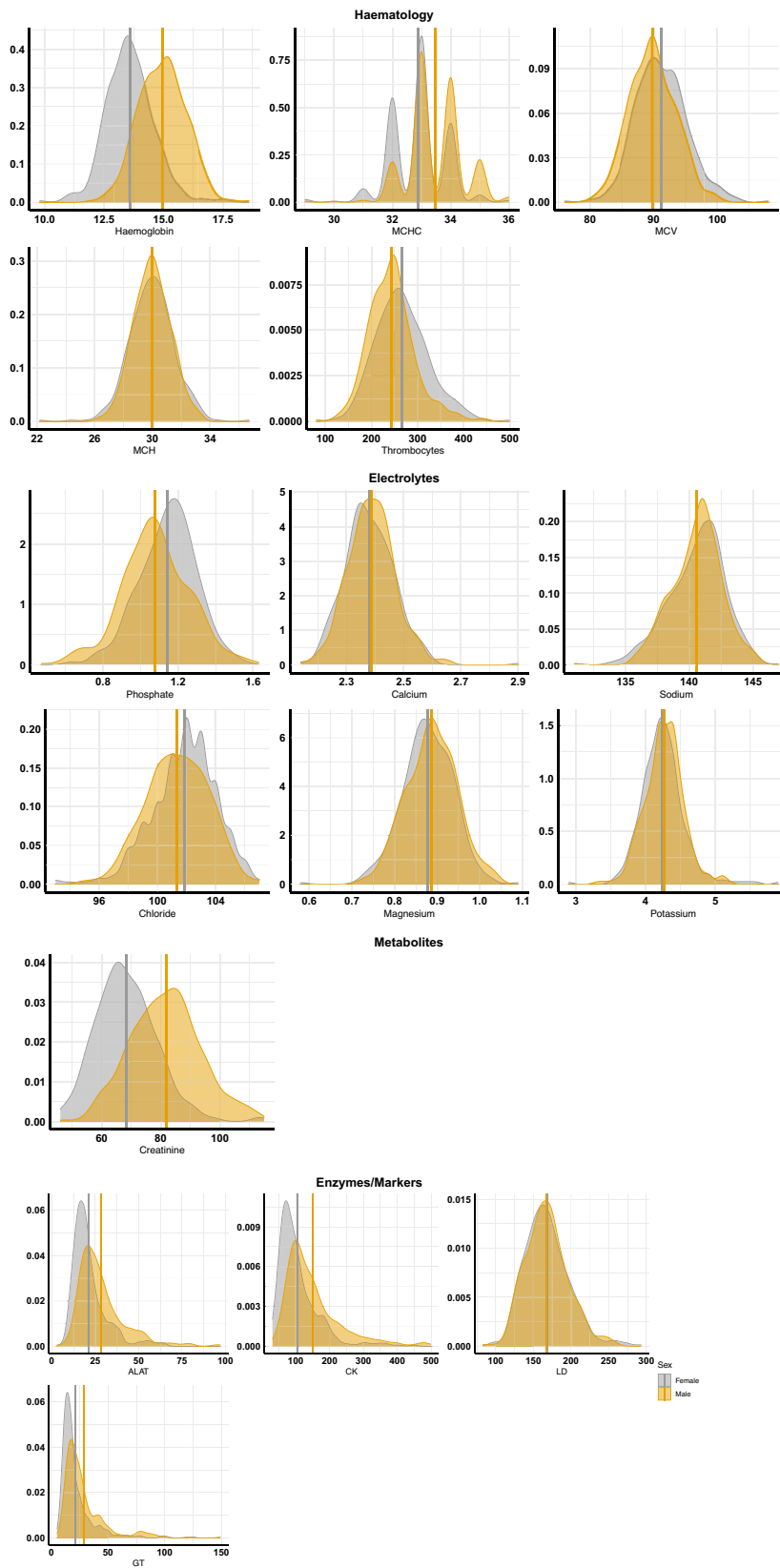


FIGURE 3 Distribution of the cardiometabolic risk factors. Density plots for each variable, split by sex (male = orange, female = grey). Vertical lines represent mean values for each sex. See Table S3 for reference (normal/healthy) range for each variable

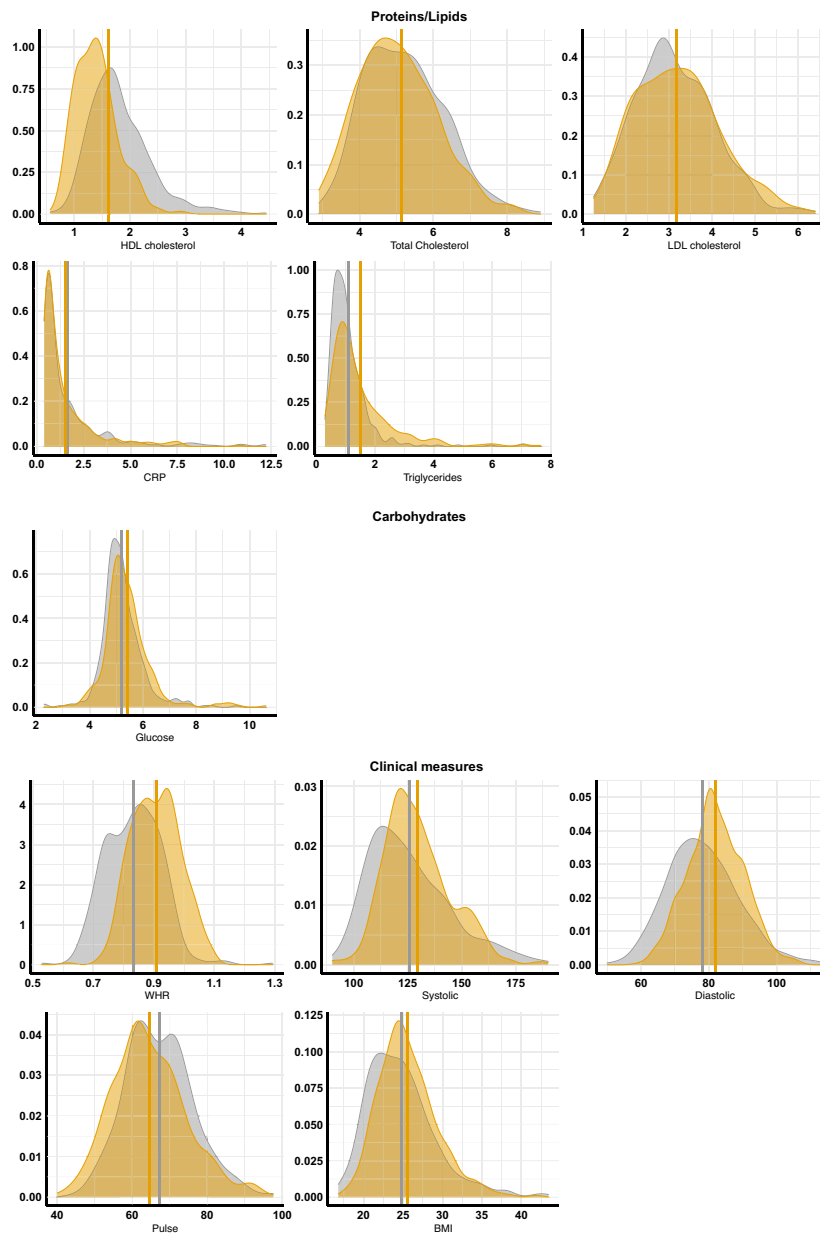


FIGURE 3 (Continued)

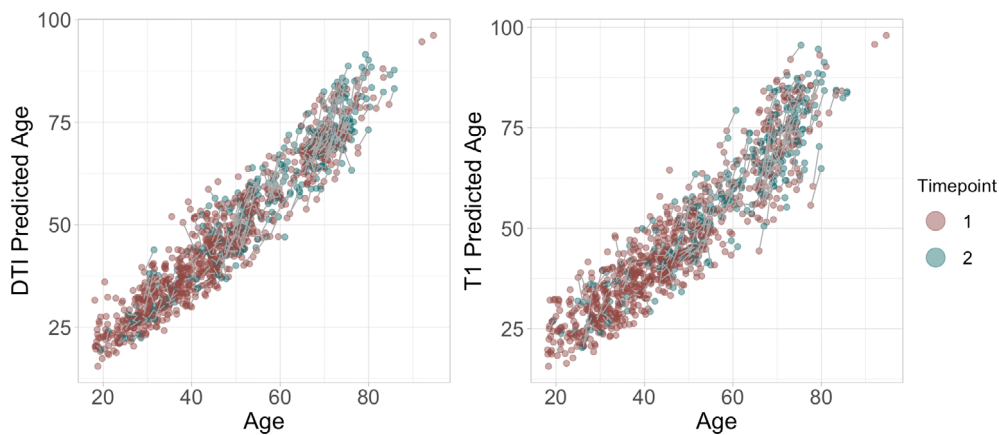


FIGURE 4 Predicted age as a function of age. The figure shows baseline brain age in red and follow up brain age in green

3 | RESULTS

3.1 | Brain age prediction

Within the training sample, the correlation between predicted and chronological age was $r = .91$ 95% CI [0.89, 0.92] for the DTI model, and $r = .90$ [0.87, 0.92] for the model based on T1-weighted data. Applying the model to the test sample resulted in a correlation between predicted and chronological age of $r = .85$ [0.83, 0.87] for the DTI model, and $r = .85$ [0.84, 0.87] for the model based on T1-weighted data. Figure S11 shows the correlations before and after age-bias correction. R^2 , RMSE, and MAE are provided in Table 2.

3.2 | Cardiometabolic risk factors

3.2.1 | Descriptive statistics

Tables 3 and 4; Figure 3.

3.3 | Bayesian multilevel models

3.3.1 | Effects of time on brain age gaps

Figure 4 shows predicted age for each model plotted as a function of age. Bayesian modeling revealed higher DTI ($\beta = 0.24$), and T1 ($\beta = 0.19$), based BAG at follow-up than baseline (Figure S12).

3.3.2 | Effects of time and age on CMRs

Figure 5 shows the posterior distributions for estimates of the coefficient for time on each variable. Full table of results for time and age effects on each variable can be seen in Table S5. Supplementary visualization of the effects of time and age on a selection of the CMRs can be seen in Figures S13–S15.

Briefly, the tests confirmed extreme evidence ($BF < 0.01$) in favor of an association between time and calcium ($\beta = -.13$), WHR ($\beta = -.10$), sodium ($\beta = .13$), chloride ($\beta = .15$), MCV ($\beta = .10$), systolic blood pressure ($\beta = -.08$), and diastolic blood pressure ($\beta = -.13$).

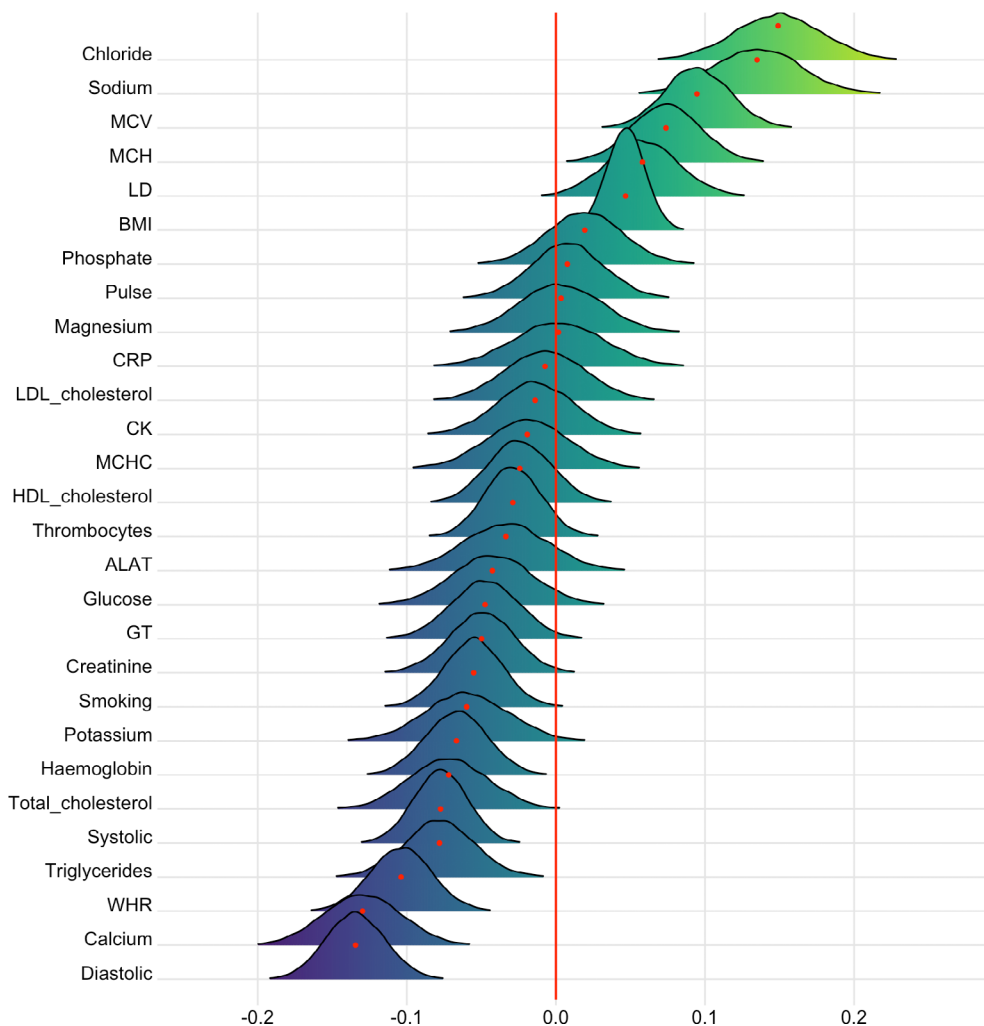


FIGURE 5 Associations between cardiometabolic risk factors and time. The figure shows posterior distributions of the estimates of the coefficient. Estimates for time on each variable with red dot in each plot representing mean value. Color scale follows direction evidence. Width of distribution represents the uncertainty of the parameter estimates

Very strong evidence was provided for BMI (BF = 0.03, β = .05), while strong evidence was provided for triglycerides (BF = 0.08, β = -.08), hemoglobin (BF = 0.07, β = -.07), and MCH (BF = 0.08, β = .08). Strong evidence was also provided in favor of no (null) association between time and pulse (BF = 11.8, β = .008), magnesium (BF = 10.8, β = .003), and LDL cholesterol (BF = 10.7, β = -.007).

Figure 6 shows the posterior distributions for estimates of the coefficient for age on each variable. The tests revealed extreme evidence (BF <0.01) in favor of an age association for phosphate (β = -.25), HDL cholesterol (β = .17), glucose (β = .25), GT (β = .21), WHR (β = .45), LD (β = .33), MCV (β = .30), MCH (β = .21), total cholesterol (β = .36), LDL cholesterol (β = 0.30), systolic (β = 0.59) and diastolic blood pressure (β = .33), potassium (β = .18), and smoking (β = .23). The models revealed moderate evidence in favor of no changes over time for thrombocytes (BF = 7.51, β = -.02), calcium (BF = 6.68, β = .03), creatinine (BF = 3.24, β = .05), and chloride (BF = 5.82, β = -.03).

3.3.3 | Associations between BAG and CMRs

Figures 7 and 8 show posterior distributions of the estimates of the coefficient reflecting the associations between each CMR and BAGs,

and Tables S6 and S7 show full table of results. Credible intervals and evidence ratios can be found in Figure S16. The tests revealed moderate evidence in favor of an association between DTI BAG and phosphate (BF = 0.17, β = .29) and MCV (BF = 0.14, β = -.32), and anecdotal evidence for WHR (BF = 0.89, β = .17), creatinine (BF = 0.6, β = .23), MCH (BF = 0.46, β = -.24), and total cholesterol (BF = 0.76, β = -.19).

Moderate evidence in favor of an association with T1 BAG was provided for systolic blood pressure (BF = 0.13, β = .37), smoking (BF = 0.17, β = .35), pulse (BF = 0.3, β = .29), and CRP (BF = 0.21, β = .29), and anecdotal evidence for BMI (BF = 0.86, β = -.20), LD (BF = 0.55, β = 0.24), and creatinine (BF = 0.52, β = -.26). No results provided moderate or stronger evidence (BF >3) in favor of the null.

3.3.4 | Interaction effects of time and CMRs on brain age gap

Figures 9 and 10 show posterior distributions reflecting estimates of the coefficient for the interaction between time and each CMRs on DTI and T1 BAGs. Tables S8 and S9 show full table of results. Credible intervals and evidence ratios can be found in Figure S17. For DTI BAG, the evidence supporting an interaction with time was strong for

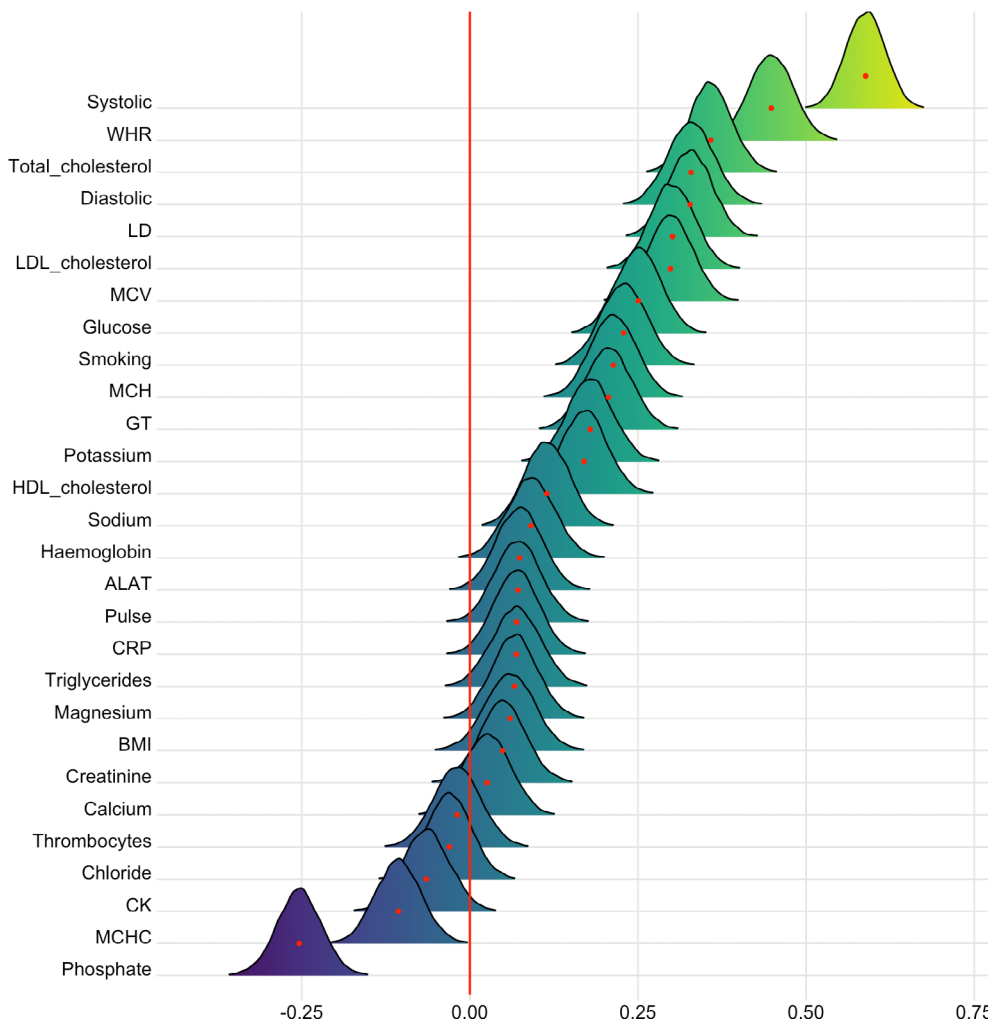
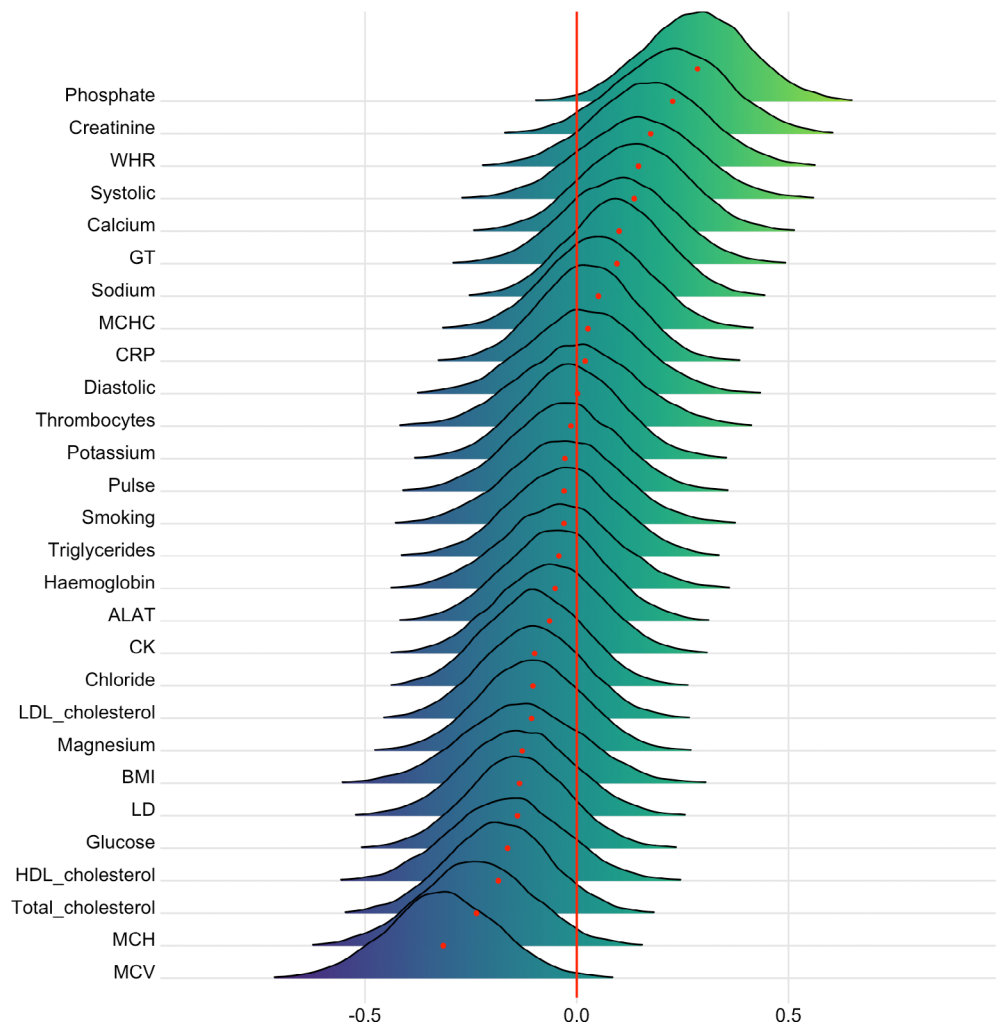


FIGURE 6 Associations between cardiometabolic risk factors and age. The figure shows posterior distributions of the estimates of the coefficient. Estimates for age on each variable

FIGURE 7 Associations between cardiometabolic risk factors and DTI BAG. The figure shows posterior distributions of the estimates of the coefficient. Estimates for each variable on DTI BAG



WHR (BF = 0.09, $\beta = .25$) and systolic blood pressure (BF = 0.07, $\beta = .25$), indicating faster pace of brain ageing among people with higher WHR and systolic blood pressure. This is visualized in Figure S18. The models further indicated moderate evidence for smoking (BF = 0.31, $\beta = .19$) and anecdotal evidence for creatinine (BF = 0.73, $\beta = .15$).

For T1 BAG, the evidence supporting an interaction with time was strong for WHR (BF = 0.06, $\beta = .30$), indicating faster pace of brain ageing among people with higher WHR. The models also revealed moderate evidence for GT (BF = 0.11, $\beta = .27$), and anecdotal for pulse (BF = 0.63, $\beta = .17$), triglycerides (BF = 0.58, $\beta = .22$), ALAT (BF = 0.37, $\beta = .23$), hemoglobin (BF = 0.64, $\beta = .18$), total cholesterol (BF = 0.72, $\beta = .17$), and LDL cholesterol (BF = 0.38, $\beta = .21$).

Thrombocytes (BF = 3.34, $\beta = -.02$), CRP (BF = 3.18, $\beta = -.01$), phosphate (BF = 3.11, $\beta = -.03$), ALAT (BF = 3.06, $\beta = -.02$), CK (BF = 3.23, $\beta = -.01$), LD (BF = 3.2, $\beta = -.01$), sodium (BF = 3.1, $\beta < .01$), chloride (BF = 3.16, $\beta = .04$), total cholesterol (BF = 3.14, $\beta = -.03$), and LDL cholesterol (BF = 3.19, $\beta = -.01$) showed moderate evidence in favor of no interaction effect with time on DTI BAG (Table S4). For T1 BAG, only MCV showed moderate evidence in favor of no association (BF = 3, $\beta < .01$).

3.3.5 | Interaction effects of age and CMRs on changes in brain age gap

Figures 11 and 12 show posterior distributions of the estimates of the coefficient for the interaction between age and each CMR on DTI and T1 BAGs. See Tables 10 and 11 for full table of results. Credible intervals and evidence ratios can be found in Figure S19. The analysis provided strong support of an interaction effect with age on DTI BAG for GT (BF = 0.09, $\beta = .36$) and systolic blood pressure (BF = 0.02, $\beta = .44$), indicating that GT and systolic blood pressure are more important predictors of brain age with increasing age. This is visualized in Figure S20. The models further indicated moderate support for WHR (BF = 0.18, $\beta = .31$), and anecdotal support for thrombocytes (BF = 0.56, $\beta = -.23$), glucose (BF = 0.36, $\beta = .24$), BMI (BF = 0.72, $\beta = .21$), CK (BF = 0.38, $\beta = -.25$), creatinine (BF = 0.4, $\beta = -.25$), diastolic blood pressure (BF = 0.51, $\beta = .23$), and potassium (BF = 0.6, $\beta = -.20$).

The support of an interaction effect with age on T1 BAG was strong for CRP (BF = 0.01, $\beta = .42$) and systolic blood pressure (BF = 0.01, $\beta = .55$), indicating that CRP and systolic blood pressure are increasingly important predictors of BAG with increasing age. The

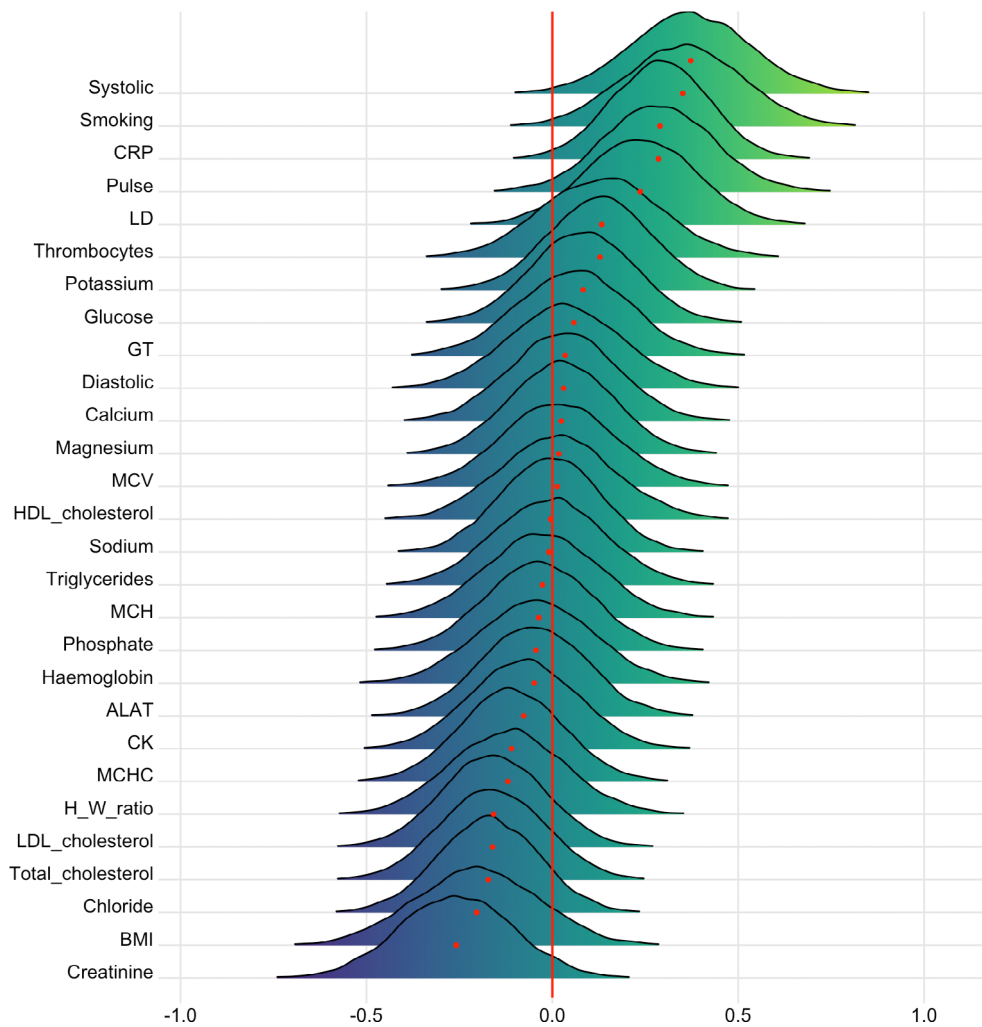


FIGURE 8 Associations between cardiometabolic risk factors and T1 BAG. The figure shows posterior distributions of the estimates of the coefficient. Estimates for each variable on T1 BAG

models further indicated moderate evidence for pulse (BF = 0.25, $\beta = .30$), glucose (BF = 0.15, $\beta = .33$), triglycerides (BF = 0.19, $\beta = .36$), WHR (BF = 0.3, $\beta = .31$), CK (BF = 0.13, $\beta = -.35$), and smoking (BF = 0.18, $\beta = .35$), and anecdotal for phosphate (BF = 0.63, $\beta = -.23$), BMI (BF = 0.67, $\beta = .24$), ALAT (BF = 0.44, $\beta = .25$), LD (BF = 0.72, $\beta = .21$), MCHC (BF = 0.41, $\beta = -.26$), MCV (BF = 0.62, $\beta = .24$), total cholesterol (BF = 0.88, $\beta = .20$), and LDL cholesterol (BF = 0.88, $\beta = .19$). No results provided moderate or stronger evidence (BF >3) in favor of the null hypothesis.

4 | DISCUSSION

Brain and cognitive ageing is highly heterogeneous and may involve a range of biological processes. Cardiometabolic risk factors are associated with increased risk of brain disorders, and a better understanding of the links between brain ageing and malleable indicators of cardiometabolic health may provide a window of opportunity for interventions. The current cross-sectional and longitudinal findings support that higher cardiometabolic risk is associated with faster brain

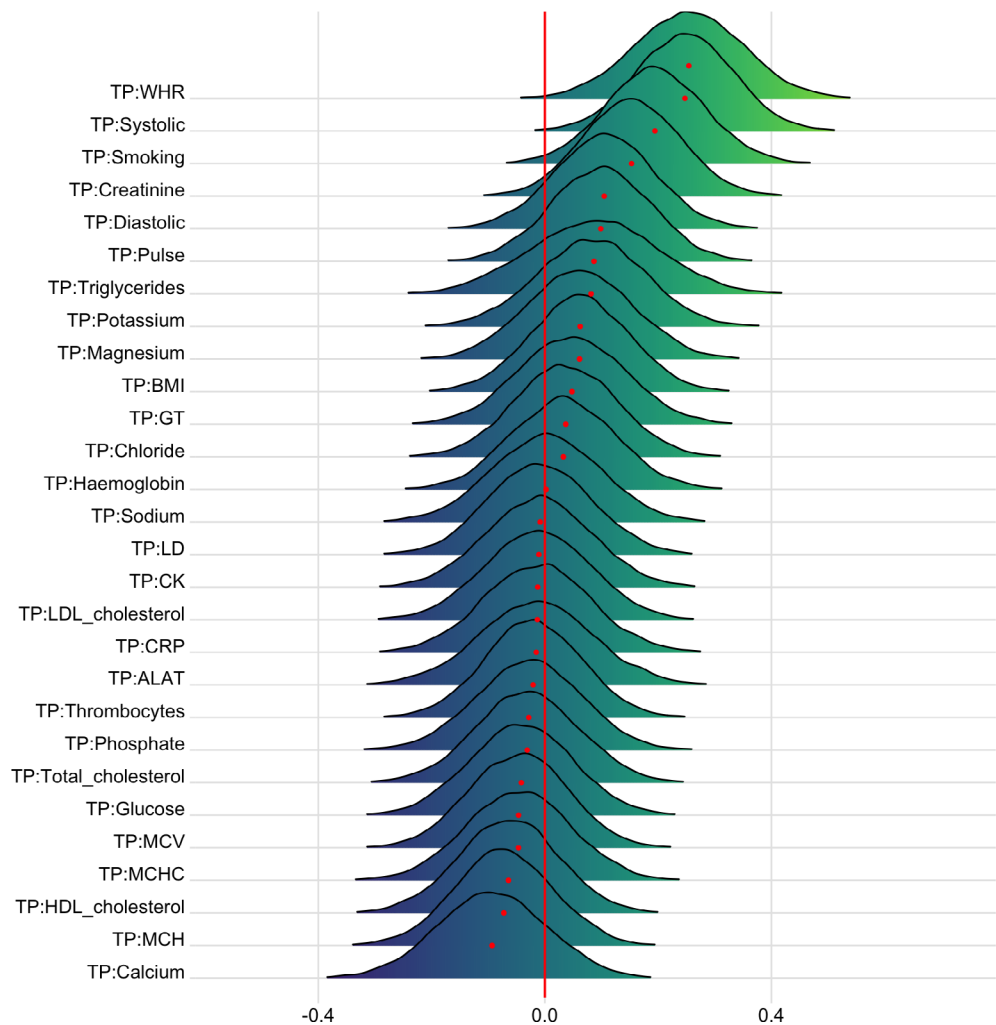
ageing. Both the overall BAG and the rates of change were associated with a range of CMRs, including anthropometric measures, blood lipids, lifestyle factors (smoking), and blood pressure.

4.1 | Associations between CMRs and age, and interactions with age

Age showed credible associations with several CMRs, including phosphate, HDL cholesterol, glucose, GT, WHR, LD, MCV, MCH, total cholesterol, LDL cholesterol, systolic and diastolic blood pressure, potassium, and smoking. Interaction effects for age and CMRs on DTI BAG were evident for GT, systolic blood pressure, and WHR. For T1 BAG, age interaction effects were evident for CRP and systolic blood pressure, pulse, triglycerides, WHR, CK, and smoking.

In general, these associations are in line with previous studies showing associations between CMR and age-related neurodegenerative diseases and cognitive decline. For example, higher serum phosphate, an element filtered by the kidney, is associated with increased

FIGURE 9 Interaction effects between cardiometabolic risk factors and time on DTI BAG. The figure shows posterior distributions of the estimates of the coefficient. Estimates for the interaction effect of time and each CMRs on DTI BAG



risk of incident dementia (Li, Xie, Bowe, Xian, & Al-Aly, 2017), and risk of brain hemorrhage (Yamada et al., 2016), while low serum phosphate level is associated with cerebral β -amyloid deposition (Park et al., 2017), increased risk of brain infarction in hemodialysis patients (Yamada et al., 2016), and lower composite score in relation to cognitive function (Basheer, Pradeep Kumar, Sreekumaran, & Ramakrishna, 2016).

Previous research has also found that high serum potassium levels were associated with MCI (Vintimilla et al., 2018), while high glucose levels were associated with low gray matter density and FA (Weinstein et al., 2015). Higher GT levels, as an index of liver function, has previously been associated with brain volume shrinkage in patients with alcohol dependence (Chen et al., 2012), brain infarcts in a healthy population (Nam et al., 2019), and cardiovascular mortality (Ruttman et al., 2005).

4.2 | Associations between CMR and brain ageing, and interactions with time

Supporting the hypothesized link between cardiometabolic risk and brain ageing, our findings demonstrated associations between several

CMRs and BAG. Strongest evidence was found for phosphate and MCV for DTI BAG, and systolic blood pressure, smoking, pulse, and CRP for T1 BAG, indicating older-appearing brains in people with poorer cardiometabolic health. Further, our longitudinal analyses revealed that the rate of brain ageing across the study period was influenced by cardiometabolic risk, with strong evidence for WHR for both BAG models, and systolic blood pressure for DTI BAG. In addition, moderate evidence of smoking was found for DTI BAG. For these effects, reduced cardiometabolic health was associated with increased rate of brain ageing.

In general, these associations are in line with previous studies showing associations between CMRs and age-related cognitive decline, with higher MCV levels being associated with reduced episodic memory, global cognitive function, and mental status (Chen et al., 2020; Gamaldo, Ferrucci, Rifkind, Longo, & Zonderman, 2014), in addition to an increased risk of cerebrovascular and cardiovascular related deaths (Wu, 2018). Moreover, related health markers of red blood cell measures (MCHC) have previously been associated with higher depressive symptom scores (Lee et al., 2017).

Higher levels of CRP, a systemic marker of inflammation, have previously been associated with smaller temporal lobes (Bettcher et al., 2012), reduced working memory, smaller cortical thickness in frontal, insula, and

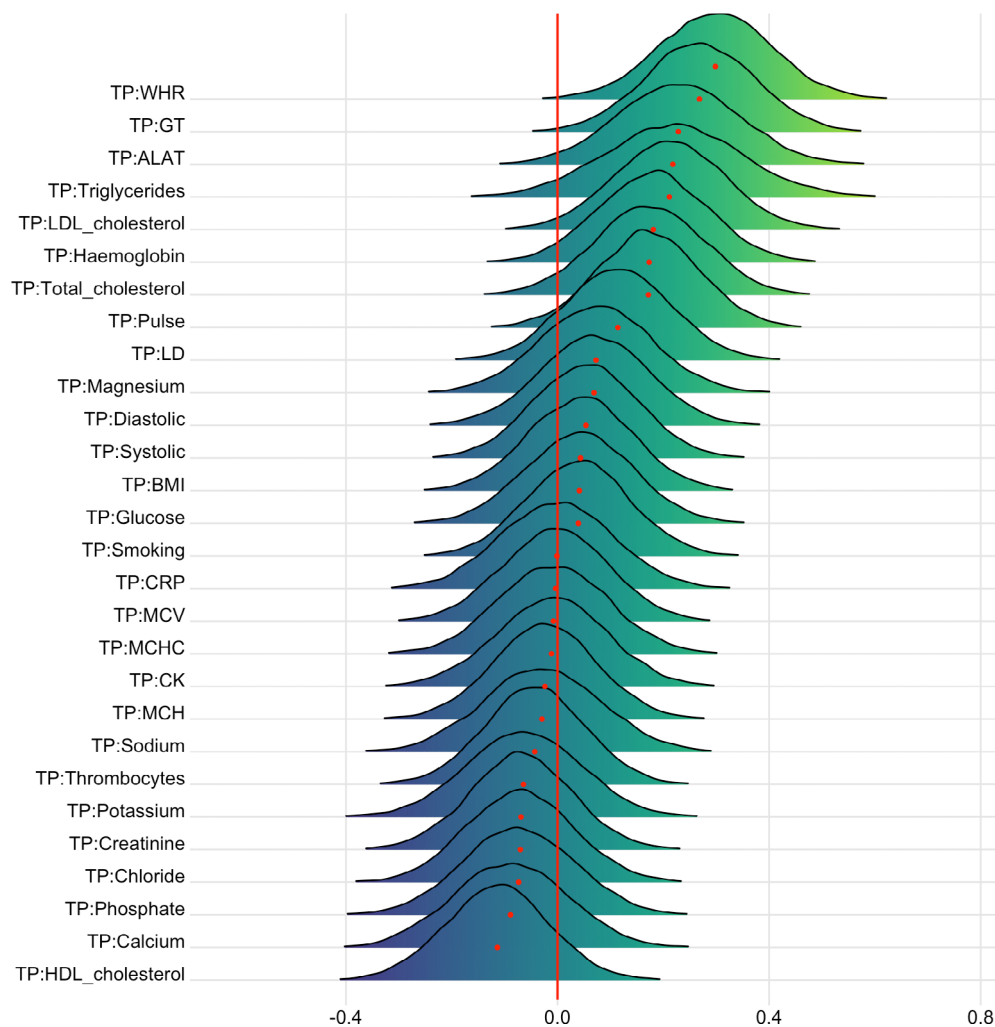


FIGURE 10 Interaction effects between cardiometabolic risk factors and time on T1 BAG. The figure shows posterior distributions of the estimates of the interaction effect of time and each variable on T1 BAG. Width of the distribution represents the uncertainty of the parameter estimates

temporal brain regions (Jacomb et al., 2018), worse performance in tests assessing executive functions, reduced global FA (Wersching et al., 2010), and increased cerebral myoinositol (Eagan et al., 2012). Although the mechanisms remain unclear, elevated CRP has also been found in patients with acute psychosis and schizophrenia (Jacomb et al., 2018).

While no direct support from studies looking at WHR and BAG currently exists, previous studies have reported associations between obesity and white matter DTI (FA and MD), white matter volume (Karlsson et al., 2013) and brain age (Kolenic et al., 2018; Ronan et al., 2016). Additionally, research investigating the association between adipose tissue and brain health has recently revealed significant negative associations between BMI and white matter surface area and cortical gray matter volume, and between WHR and caudate volume (Gurholt et al., 2020).

Our results demonstrating that elevated systolic blood pressure and smoking were associated with faster brain ageing over time are in line with previous cross-sectional studies, with systolic blood pressure reportedly being associated with white matter BAG (de Lange et al., 2020) and reduced cerebral vascular density (Williamson et al., 2018). Similarly, smoking has also been associated with decreased total brain volume (Reiman et al., 2008) and reduced cerebral vascular density (Williamson et al., 2018). Moreover, longitudinal

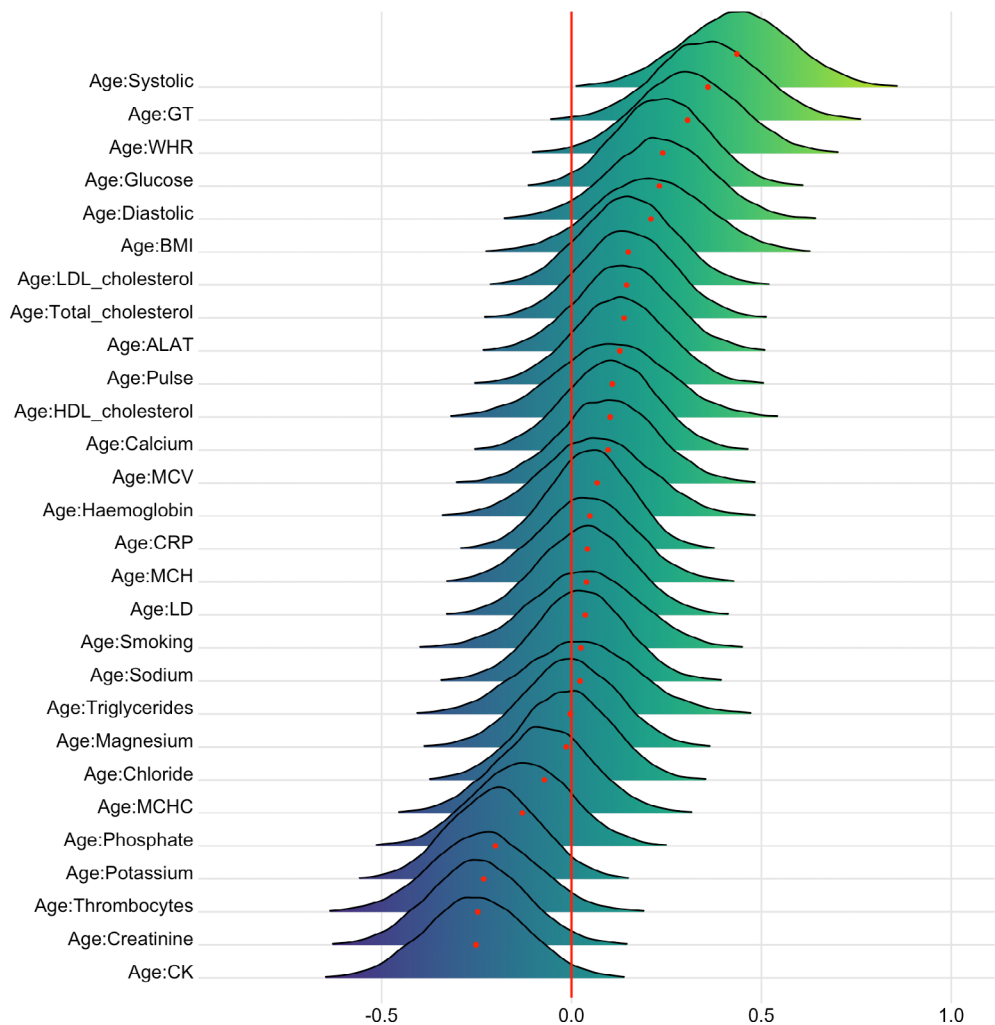
studies have reported higher rates of annual white matter lesion progression in subjects with increased systolic blood pressure (Verhaaren et al., 2013).

Albeit with moderate evidence, the rate of brain ageing was also associated with increased pulse and several key blood biomarkers reflecting various aspects of cardiometabolic health, including creatinine, GT, triglycerides, ALAT, total and LDL cholesterol, and hemoglobin. These findings jointly contribute to the larger picture of modifiable CMRs influencing brain ageing. Additionally, the findings are largely in line with previous studies demonstrating more white matter hyperintensities in people with lower hemoglobin levels, and less coherent white matter in people with high total and LDL cholesterol and high triglyceride levels (Williams et al., 2013).

4.3 | Future research and recommendations for treatment

In common with other imaging based surrogate markers, brain predicted age should be understood as not only a phenomenon impacted by the effects of ageing, but also by the effects of a lifetime of exposure to positive and negative lifestyles and environments,

FIGURE 11 Interaction effects between cardiometabolic risk factors and age on DTI BAG. The figure shows posterior distributions of the estimates for the interaction effect between age and each variable on DTI BAG, with red dot representing mean value. Width of the distribution represents the uncertainty of the parameter estimates



coupled with a genetic component that plays a crucial role in the variation. Despite not being able to disentangle the contribution of each of these components when looking at an individual's predicted age and subsequent brain age gap, this disparity between chronological and predicted age still provides us with an individualized marker of deviation from the expected value. And with this, recommendations for treatment can focus on the individual and target management of risk.

Alternatively, early intervention strategies that place their focus on prevention rather than management of risk may be more beneficial. For example, Williamson et al. (2018) found that cardiovascular health in early adulthood relates to brain atrophy in later life. McEvoy et al. (2015) found that white matter alterations appear early in the course of hypertension and may persist despite adequate treatment. The implication of this suggests that preventive strategies that promote cardiometabolic health early may be more beneficial in prolonging healthy brain ageing. Moreover, maintaining the structure of the brain in a younger state may have profound effects on delaying the onset of age-related neurodegenerative diseases and cognitive decline (Qiu & Fratiglioni, 2015; Steffener, 2016). While the current longitudinal study focuses on cardiometabolic risk factors, previous cross-sectional results from a partly overlapping sample has shown

poorer performance on cognitive tests in individuals with an over-estimated age (Richard et al., 2018). Future research may aim to integrate cardiometabolic risk factors with both brain imaging data and crude measures of cognitive ability in a longitudinal context. Informed by studies showing that higher levels of physical exercise (Steffener, 2016) and meditation (Luders, Cherbun, & Gaser, 2016) are associated with lower brain ageing, interacting with modifiable CMRs may change risk trajectories and prevent progression to disease for a manifold of cardiovascular and neurodegenerative diseases as well as mental disorders (Ringen et al., 2018; Ringen, Engh, Birkenaes, Dieset, & Andreassen, 2014; Schmitt et al., 2018).

4.4 | Strengths and limitations

The current study had several strengths. As there is both variability in the brain ageing process from person to person (Aycheh et al., 2018), and variability in CMRs, the current study benefitted from a mixed cross-sectional and longitudinal design, whereby changes can be tracked across timepoints. For brain age, the prediction models had high accuracy, and separate diffusion and T1-weighted brain age gaps provided insight into modality-specific impact of CMRs. Most brain-

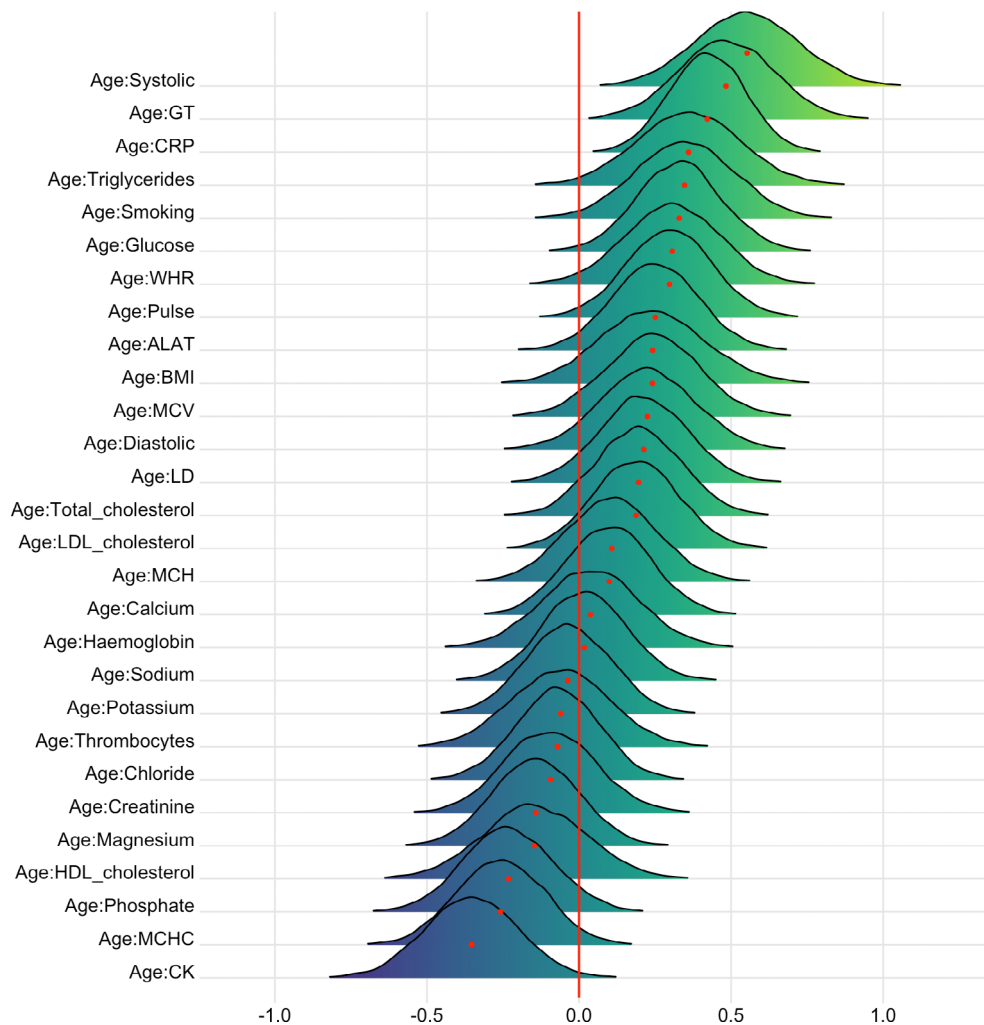


FIGURE 12 Interaction effects between cardiometabolic risk factors and age on T1 BAG. The figure shows posterior distributions of the estimates for the interaction effect between age and each variable on T1 BAG, with red dot representing mean value. Width of the distribution represents the uncertainty of the parameter estimate

age models use only T1-weighted structural MRI but changes in white matter microstructure and coherence may precede alterations that may not be detected by T1-weighted MRI (Cole, 2020).

Some limitations must also be addressed. The use of brain age prediction for generating imaging-based biomarkers continue to be extended and developed (Anatürk et al., 2021; Franke & Gaser, 2019; Peng, Gong, Beckmann, Vedaldi, & Smith, 2019; Smith, Vidaurre, Alfaro-Almagro, Nichols, & Miller, 2019). While several methods for age-bias correction have been proposed (Beheshti et al., 2019; Liang et al., 2019; Smith et al., 2019), many of these methods provide equivalent results (de Lange et al., 2021; de Lange & Cole, 2020). Adjusting for age-bias is not straight-forward as it can in some cases lead to inflated values, particularly in datasets with a narrow age range where the variation is small (de Lange et al., 2021). Improving methods for age bias (Treder et al., 2021) or incorporating uncertainties into the predictions (Hahn et al., 2021; Marquand et al., 2019) represent promising developments toward robust markers for brain health and disease. Another limitation is that the sample is predominantly ethnic Northern European/Scandinavian, restricting our ability to generalize to the wider public and other population groups of generally higher or lower risk than our sample. Moreover, the sample is generally healthy, and biases due to nonrandom attrition could be introduced.

Contrarily, the range of the values for many blood test and pressure measurements reveal incidental indication of possible kidney failure, anaemia, platelet disorder, hyperlipidaemia, and hypertension. Future studies should utilize a more comprehensive cardiometabolic risk assessment detailing dietary routines, alcohol intake, psychosocial stress, and physical activity, which jointly have been shown to account for 90% of the population-attributable risk of myocardial infarction in men and 94% in women (Yusuf, Hawken, & Ounpuu, 2005). With these limitations in mind, a degree of scepticism toward relating the results clinically is warranted, as some results may be driven by temporary physiological variations and food intake prior to blood testing. Additionally, scepticism is warranted regarding the specificity of the findings given that many of the CMRs included in the study are related to each other to some degree. While very few CMRs reveal correlation coefficients that indicate multicollinearity, there may still be some redundancy of different variables showing the same information or the estimate of a predictor being less precise. Structural specificity must also be considered, as supplementary analysis revealed a correlation between T1 and DTI BAG (Figure S22). Future research could consider relatedness of measures by adopting approaches that model complex relationships among variables better (Wang et al., 2020).

The longitudinal aspect of the study must also be discussed. Although the FreeSurfer longitudinal stream was carried out for both cross sectional and longitudinal data to avoid thickness estimates—and consequently T1 BAG—being influenced for follow up data, recent research suggests number of acquisitions per individual has an impact on the function of the FreeSurfer longitudinal pipeline (Beare et al., 2021). Further, the imputation procedure (MICE) was originally proposed for cross-sectional data, and while not in the scope of this study, more complex imputation methods that explicitly reflect the longitudinal structure of analysis models may be of interest for future studies. Last, the study may be limited due to a mean interval of 19.7 months for only one follow-up. Long-term longitudinal studies with several follow up sessions will be required to determine the temporal course and clinical predictive value of our findings in relation to future cardiometabolic disease and brain ageing.

The findings provide further support to the notion of the BAG reflecting individual variation in brain ageing (de Lange et al., 2020; Niu et al., 2020). While the modality-specific grey and white matter models showed similar performance, T1- and DTI-based BAGs revealed different associations with various CMRs. While it is likely that tissue specific brain age models capture biologically distinct information beyond single-modality models (de Lange et al., 2020; Richard et al., 2018; Smith et al., 2020), future research should look into additional regional modeling of tissue-specific brain ageing to detect associations with CMRs and other health indicators.

4.5 | Conclusion

Our findings support that cardiometabolic risk factors including systolic blood pressure, WHR, and smoking, are associated with an older-appearing brain and accelerated brain ageing. While evidence demonstrating that effective management of modifiable CMRs reduces severity of associated brain imaging abnormalities is needed, promotion of improved cardiometabolic health and increasing existing knowledge on the links between the structure and function of the brain and cardiometabolic health can aid the development of preventative and risk-management treatment strategies in the general population and, likely, among patients with neurodegenerative and mental disorders.

ACKNOWLEDGMENTS

The study is supported by the Research Council of Norway (223273, 249795, 248238, 276082), the South-Eastern Norway Regional Health Authority (2014097, 2015044, 2015073, 2016083, 2018037, 2018076), the Norwegian ExtraFoundation for Health and Rehabilitation (2015/FO5146), KG Jebsen Stiftelsen, Swiss National Science Foundation (grant PZ00P3_193658), German Federal Ministry of Education and Research (BMBF, grant O1ZX1904A), ERA-Net Cofund through the ERA PerMed project “IMPLEMENT” (Research Council of Norway—298646), and the European Research Council under the European Union's Horizon 2020 Research and Innovation program

(ERC StG, Grant # 802998 and RIA Grant # 847776). Open access funding enabled and organized by Projekt DEAL.

DATA AVAILABILITY STATEMENT

The data and code used in the study is freely available in a public repository (Open Science Framework) and accessible through the “data and code” section of the bioRxiv preprint (<https://www.medrxiv.org/content/10.1101/2021.02.25.2125272v1>), or directly through the OSF webpage (<https://osf.io/ujwat/>).

ORCID

Dani Beck  <https://orcid.org/0000-0002-0974-9304>

Irene Voldsbekk  <https://orcid.org/0000-0001-9393-5857>

Geneviève Richard  <https://orcid.org/0000-0001-6475-2576>

Lars T. Westlye  <https://orcid.org/0000-0001-8644-956X>

REFERENCES

- Anatürk, M., Kaufmann, T., Cole, J. H., Suri, S., Griffanti, L., Zsoldos, E., ... de Lange, A.-M. G. (2021). Prediction of brain age and cognitive age: Quantifying brain and cognitive maintenance in aging. *Human Brain Mapping, 42*(6), 1626–1640. <https://doi.org/10.1002/hbm.25316>
- Andersson, J. L. R., & Sotiropoulos, S. N. (2016). An integrated approach to correction for off-resonance effects and subject movement in diffusion MR imaging. *NeuroImage, 125*, 1063–1078. <https://doi.org/10.1016/j.neuroimage.2015.10.019>
- Aycheh, H. M., Seong, J.-K., Shin, J.-H., Na, D. L., Kang, B., Seo, S. W., & Sohn, K.-A. (2018). Biological brain age prediction using cortical thickness data: A large scale cohort study. *Frontiers in Aging Neuroscience, 10*, 252. <https://doi.org/10.3389/fnagi.2018.00252>
- Basheer, M. P., Pradeep Kumar, K. M., Sreekumaran, E., & Ramakrishna, T. (2016). A study of serum magnesium, calcium and phosphorus level, and cognition in the elderly population of South India. *Alexandria Journal of Medicine, 52*(4), 303–308. <https://doi.org/10.1016/j.ajme.2015.11.001>
- Beare, R., Yang, J. Y.-M., Ball, G., Moran, C., Srikanth, V., & Seal, M. (2021). Participant followup rate can bias structural imaging measures in longitudinal studies. *BioRxiv*. <https://doi.org/10.1101/2021.02.10.430674>
- Beck, D., de Lange, A.-M., Maximov, I. I., Richard, G., Andreassen, O. A., Nordvik, J. E., & Westlye, L. T. (2021). White matter microstructure across the adult lifespan: A mixed longitudinal and cross-sectional study using advanced diffusion models and brain-age prediction. *NeuroImage, 224*, 117441. <https://doi.org/10.1016/j.neuroimage.2020.117441>
- Beheshti, I., Nugent, S., Potvin, O., & Duchesne, S. (2019). Bias-adjustment in neuroimaging-based brain age frameworks: A robust scheme. *NeuroImage: Clinical, 24*, 102063. <https://doi.org/10.1016/j.nicl.2019.102063>
- Bettcher, B. M., Wilhelm, R., Rigby, T., Green, R., Miller, J. W., Racine, C. A., ... Kramer, J. H. (2012). C-reactive protein is related to memory and medial temporal brain volume in older adults. *Brain, Behavior, and Immunity, 26*(1), 103–108. <https://doi.org/10.1016/j.bbi.2011.07.240>
- Bürkner, P.-C. (2017). brms: An R package for bayesian multilevel models using stan. *Journal of Statistical Software, 80*(1). <https://doi.org/10.18637/jss.v080.i01>
- Bürkner, P.-C. (2018). Advanced bayesian multilevel modeling with the R package brms. *The R Journal, 10*(1), 395–411. <https://doi.org/10.32614/RJ-2018-017>
- Chen, C.-H., Walker, J., Momenan, R., Rawlings, R., Heilig, M., & Hommer, D. W. (2012). Relationship between liver function and brain shrinkage in patients with alcohol dependence: Relationship between

- liver function and brain shrinkage. *Alcoholism: Clinical and Experimental Research*, 36(4), 625–632. <https://doi.org/10.1111/j.1530-0277.2011.01662.x>
- Chen, Y., Ma, C. N., Luo, L., Yin, J., Gao, Z., Yu, Z., & Wan, Z. (2020). The cross-sectional association between mean corpuscular volume level and cognitive function in Chinese over 45 years old: Evidence from the China health and retirement longitudinal study. *PLOS ONE*, 15(12), e0243227. <http://dx.doi.org/10.1371/journal.pone.0243227>
- Cole, J. H. (2020). Multimodality neuroimaging brain-age in UK biobank: Relationship to biomedical, lifestyle, and cognitive factors. *Neurobiology of Aging*, 92, 34–42. <https://doi.org/10.1016/j.neurobiolaging.2020.03.014>
- Cole, J. H., Poudel, R. P. K., Tsagkrasoulis, D., Caan, M. W. A., Steves, C., Spector, T. D., & Montana, G. (2017). Predicting brain age with deep learning from raw imaging data results in a reliable and heritable biomarker. *NeuroImage*, 163, 115–124. <https://doi.org/10.1016/j.neuroimage.2017.07.059>
- Cole, J. H., Ritchie, S. J., Bastin, M. E., Hernández, M. C. V., Maniega, S. M., Royle, N., ... Deary, I. J. (2018). Brain age predicts mortality. *Molecular Psychiatry*, 23(5), 1385–1392. <https://doi.org/10.1038/mp.2017.62>
- de Lange, A.-M. G., & Cole, J. H. (2020). Commentary: Correction procedures in brain-age prediction. *NeuroImage: Clinical*, 26, 102229. <https://doi.org/10.1016/j.nicl.2020.102229>
- de Lange, A.-M. G., Anatórk, M., Suri, S., Kaufmann, T., Cole, J. H., Griffanti, L., ... Ebmeier, K. I. P. (2020). Multimodal brain-age prediction and cardiovascular risk: The Whitehall II MRI sub-study. *NeuroImage*, 222, 117292. <http://dx.doi.org/10.1016/j.neuroimage.2020.117292>
- de Lange, A.-M.G., Barth, C., Kaufmann, T., Maximov, I. I., Meer, D., Agartz, I., Westlye, L. T. (2020). Women's brain aging: Effects of sex-hormone exposure, pregnancies, and genetic risk for Alzheimer's disease. *Human Brain Mapping*, 41(18), 5141–5150. <http://dx.doi.org/10.1002/hbm.25180>
- de Lange, A.-M. G., Anatórk, M., Rokicki, J., Han, L. K. M., Franke, K., Alnæs, D., ... Cole, J. H. (2021). Mind the gap: Performance metric evaluation in brain-age prediction. *BioRxiv*. <https://doi.org/10.1101/2021.05.16.444349>
- de Lange, A.-M. G., Kaufmann, T., van der Meer, D., Maglanoc, L. A., Alnæs, D., Moberget, T., ... Westlye, L. T. (2019). Population-based neuroimaging reveals traces of childbirth in the maternal brain. *Proceedings of the National Academy of Sciences*, 116(44), 22341–22346. <https://doi.org/10.1073/pnas.1910666116>
- Desikan, R. S., Ségonne, F., Fischl, B., Quinn, B. T., Dickerson, B. C., Blacker, D., ... Killiany, R. J. (2006). An automated labeling system for subdividing the human cerebral cortex on MRI scans into gyral based regions of interest. *NeuroImage*, 31(3), 968–980. <https://doi.org/10.1016/j.neuroimage.2006.01.021>
- Eagan, D. E., Gonzales, M. M., Tarumi, T., Tanaka, H., Stautberg, S., & Haley, A. P. (2012). Elevated serum C-reactive protein relates to increased cerebral myoinositol levels in middle-aged adults. *Cardiovascular Psychiatry and Neurology*, 2012, 1–9. <https://doi.org/10.1155/2012/120540>
- Filzmoser, P., Garrett, R. G., & Reimann, C. (2005). Multivariate outlier detection in exploration geochemistry. *Computers & Geosciences*, 31(5), 579–587.
- Fischl, B., Salat, D. H., Busa, E., Albert, M., Dieterich, M., Haselgrove, C., ... Dale, A. M. (2002). Whole brain segmentation. *Neuron*, 33(3), 341–355. [https://doi.org/10.1016/S0896-6273\(02\)00569-X](https://doi.org/10.1016/S0896-6273(02)00569-X)
- Franke, K., & Gaser, C. (2019). Ten years of BrainAGE as a neuroimaging biomarker of brain aging: What insights have we gained? *Frontiers in Neurology*, 10, 789. <https://doi.org/10.3389/fneur.2019.00789>
- Franke, K., Gaser, C., Manor, B., & Novak, V. (2013). Advanced BrainAGE in older adults with type 2 diabetes mellitus. *Frontiers in Aging Neuroscience*, 5, 90. <http://dx.doi.org/10.3389/fnagi.2013.00090>
- Franke, K., Ristow, M., & Gaser, C. (2014). Gender-specific impact of personal health parameters on individual brain aging in cognitively unimpaired elderly subjects. *Frontiers in Aging Neuroscience*, 6, 94. <https://doi.org/10.3389/fnagi.2014.00094>
- Franke, K., Ziegler, G., Klöppel, S., & Gaser, C. (2010). Estimating the age of healthy subjects from T1-weighted MRI scans using kernel methods: Exploring the influence of various parameters. *NeuroImage*, 50(3), 883–892. <https://doi.org/10.1016/j.neuroimage.2010.01.005>
- Friedman, J. I., Tang, C. Y., de Haas, H. J., Changchien, L., Goliasch, G., Dabas, P., ... Narula, J. (2014). Brain imaging changes associated with risk factors for cardiovascular and cerebrovascular disease in asymptomatic patients. *JACC. Cardiovascular Imaging*, 7(10), 1039–1053. <https://doi.org/10.1016/j.jcmg.2014.06.014>
- Fuhrmann, D., Nesbitt, D., Shafto, M., Rowe, J. B., Price, D., Gadie, A., ... Willis, L. (2019). Strong and specific associations between cardiovascular risk factors and white matter micro- and macrostructure in healthy aging. *Neurobiology of Aging*, 74, 46–55. <https://doi.org/10.1016/j.neurobiolaging.2018.10.005>
- Gamaldo, A. A., Ferrucci, L., Rifkind, J., Longo, D. L., & Zonderman, A. B. (2014). The relationship between mean corpuscular volume and cognitive performance in older adults. *Journal of the American Geriatrics Society*, 61(1), 84–89.
- Gurholt, T. P., Kaufmann, T., Frei, O., Alnæs, D., Haukvik, U. K., van der Meer, D., ... Andreassen, O. A. (2021). Population-based body-brain mapping links brain morphology with anthropometrics and body composition. *Translational Psychiatry*, 11(1). <http://dx.doi.org/10.1038/s41398-021-01414-7>
- Hahn, T., Fisch, L., Ernsting, J., Winter, N. R., Leenings, R., Sarink, K., ... Dannlowski, U. (2021). From 'loose fitting' to high-performance, uncertainty-aware brain-age modelling. *Brain*, 144(3), e31. <https://doi.org/10.1093/brain/awaa454>
- Han, L. K. M., Dinga, R., Hahn, T., Ching, C. R. K., Eyler, L. T., Aftanas, L., ... Schmaal, L. (2020). Brain aging in major depressive disorder: Results from the ENIGMA major depressive disorder working group. *Molecular Psychiatry*, 1–16. <https://doi.org/10.1038/s41380-020-0754-0>
- Høgestøl, E. A., Kaufmann, T., Nygaard, G. O., Beyer, M. K., Sowa, P., Nordvik, J. E., ... Westlye, L. T. (2019). Cross-sectional and longitudinal mri brain scans reveal accelerated brain aging in multiple sclerosis. *Frontiers in Neurology*, 10, 450. <https://doi.org/10.3389/fneur.2019.00450>
- Hoogenboom, W. S., Marder, T. J., Flores, V. L., Huisman, S., Eaton, H. P., Schneiderman, J. S., ... Musen, G. (2014). Cerebral white matter integrity and resting-state functional connectivity in middle-aged patients with type 2 diabetes. *Diabetes*, 63(2), 728–738. <https://doi.org/10.2337/db13-1219>
- Hsu, J.-L., Chen, Y.-L., Leu, J.-G., Jaw, F.-S., Lee, C.-H., Tsai, Y.-F., ... Leemans, A. (2012). Microstructural white matter abnormalities in type 2 diabetes mellitus: A diffusion tensor imaging study. *NeuroImage*, 59(2), 1098–1105. <https://doi.org/10.1016/j.neuroimage.2011.09.041>
- Hua, K., Zhang, J., Wakana, S., Jiang, H., Li, X., Reich, D. S., ... Mori, S. (2008). Tract probability maps in stereotaxic spaces: Analyses of white matter anatomy and tract-specific quantification. *NeuroImage*, 39(1), 336–347. <https://doi.org/10.1016/j.neuroimage.2007.07.053>
- Jacomb, I., Stanton, C., Vasudevan, R., Powell, H., O'Donnell, M., Lenroot, R., ... Weickert, T. W. (2018). C-reactive protein: Higher during acute psychotic episodes and related to cortical thickness in schizophrenia and healthy controls. *Frontiers in Immunology*, 9, 2230. <https://doi.org/10.3389/fimmu.2018.02230>
- Jeerakathil, T., Wolf, P. A., Beiser, A., Massaro, J., Seshadri, S., D'Agostino, R. B., & DeCarli, C. (2004). Stroke risk profile predicts white matter hyperintensity volume: The Framingham study. *Stroke*, 35(8), 1857–1861. <https://doi.org/10.1161/01.STR.0000135226.53499.85>
- Jenkinson, M., Beckmann, C. F., Behrens, T. E. J., Woolrich, M. W., & Smith, S. M. (2012). FSL. *NeuroImage*, 62(2), 782–790. <https://doi.org/10.1016/j.neuroimage.2011.09.015>

- Karlsson, H. K., Tuulari, J. J., Hirvonen, J., Lepomäki, V., Parkkola, R., Hiltunen, J., ... Nummenmaa, L. (2013). Obesity is associated with white matter atrophy: A combined diffusion tensor imaging and voxel-based morphometric study: Obesity is associated with white matter atrophy. *Obesity*, 21(12), 2530–2537. <https://doi.org/10.1002/oby.20386>
- Kaufmann, T., van der Meer, D., Doan, N. T., Schwarz, E., Lund, M. J., Agartz, I., ... Westlye, L. T. (2019). Common brain disorders are associated with heritable patterns of apparent aging of the brain. *Nature Neuroscience*, 22(10), 1617–1623. <https://doi.org/10.1038/s41593-019-0471-7>
- Kellner, E., Dhital, B., Kiselev, V. G., & Reiser, M. (2016). Gibbs-ringing artifact removal based on local subvoxel-shifts. *Magnetic Resonance in Medicine*, 76(5), 1574–1581. <https://doi.org/10.1002/mrm.26054>
- Kolenic, M., Franke, K., Hlinka, J., Matejka, M., Capkova, J., Pausova, Z., ... Hajek, T. (2018). Obesity, dyslipidemia and brain age in first-episode psychosis. *Journal of Psychiatric Research*, 99, 151–158. <https://doi.org/10.1016/j.jpsychires.2018.02.012>
- Kuhn, T., Kaufmann, T., Doan, N. T., Westlye, L. T., Jones, J., Nunez, R. A., ... Thames, A. D. (2018). An augmented aging process in brain white matter in HIV. *Human Brain Mapping*, 39(6), 2532–2540. <https://doi.org/10.1002/hbm.24019>
- Lee, J.-M., Nadimpalli, S. B., Yoon, J.-H., Mun, S. Y., Suh, I., & Kim, H. C. (2017). Association between mean corpuscular hemoglobin concentration and future depressive symptoms in women. *The Tohoku Journal of Experimental Medicine*, 241(3), 209–217. <https://doi.org/10.1620/tjem.241.209>
- Li, T., Xie, Y., Bowe, B., Xian, H., & Al-Aly, Z. (2017). Serum phosphorus levels and risk of incident dementia. *PLoS One*, 12(2), e0171377. <https://doi.org/10.1371/journal.pone.0171377>
- Liang, H., Zhang, F., & Niu, X. (2019). Investigating systematic bias in brain age estimation with application to post-traumatic stress disorders. *Human Brain Mapping*, 40, 3143–3152. <https://doi.org/10.1002/hbm.24588>
- Lindenberger, U. (2014). Human cognitive aging: Corriger la fortune? *Science*, 346(6209), 572–578. <https://doi.org/10.1126/science.1254403>
- Luders, E., Cherbuin, N., & Gaser, C. (2016). Estimating brain age using high-resolution pattern recognition: Younger brains in long-term meditation practitioners. *NeuroImage*, 134, 508–513. <https://doi.org/10.1016/j.neuroimage.2016.04.007>
- Marquand, A. F., Kia, S. M., Zabihi, M., Wolfers, T., Buitelaar, J. K., & Beckmann, C. F. (2019). Conceptualizing mental disorders as deviations from normative functioning. *Molecular Psychiatry*, 24(10), 1415–1424. <https://doi.org/10.1038/s41380-019-0441-1>
- Maximov, I. I., Alnæs, D., & Westlye, L. T. (2019). Towards an optimised processing pipeline for diffusion magnetic resonance imaging data: Effects of artefact corrections on diffusion metrics and their age associations in UK Biobank. *Human Brain Mapping*, 40(14), 4146–4162. <https://doi.org/10.1002/hbm.24691>
- McEvoy, L. K., Fennema-Notestine, C., Eyer, L. T., Franz, C. E., Hagler, D. J., Lyons, M. J., ... Kremen, W. S. (2015). Hypertension-related alterations in white matter microstructure detectable in middle age. *Hypertension*, 66(2), 317–323. <https://doi.org/10.1161/HYPERTENSIONAHA.115.05336>
- Murray, A. D., Staff, R. T., Shenkin, S. D., Deary, I. J., Starr, J. M., & Whalley, L. J. (2005). Brain white matter hyperintensities: Relative importance of vascular risk factors in nondemented elderly people. *Radiology*, 237(1), 251–257. <https://doi.org/10.1148/radiol.2371041496>
- Nam, K.-W., Kwon, H.-M., Jeong, H.-Y., Park, J.-H., Kim, S. H., & Jeong, S.-M. (2019). Serum gamma-glutamyl transferase is associated with silent brain infarcts in a healthy population. *Atherosclerosis*, 280, 45–50. <https://doi.org/10.1016/j.atherosclerosis.2018.11.005>
- Niu, X., Zhang, F., Kounios, J., & Liang, H. (2020). Improved prediction of brain age using multimodal neuroimaging data. *Human Brain Mapping*, 41(6), 1626–1643. <http://dx.doi.org/10.1002/hbm.24899>
- Pardoe, H. R., Cole, J. H., Blackmon, K., Thesen, T., & Kuzniecky, R. (2017). Structural brain changes in medically refractory focal epilepsy resemble premature brain aging. *Epilepsy Research*, 133, 28–32. <https://doi.org/10.1016/j.eplepsyres.2017.03.007>
- Park, J.-C., Han, S.-H., Byun, M. S., Yi, D., Lee, J. H., Park, K., ... Mook-Jung, I. (2017). Low serum phosphorus correlates with cerebral A β deposition in cognitively impaired subjects: Results from the KBASE study. *Frontiers in Aging Neuroscience*, 9, 362. <https://doi.org/10.3389/fnagi.2017.00362>
- Peng, H., Gong, W., Beckmann, C. F., Vedaldi, A., & Smith, S. M. (2021). Accurate brain age prediction with lightweight deep neural networks. *Medical Image Analysis*, 68, 101871. <http://dx.doi.org/10.1016/j.media.2020.101871>
- Perry, B. I., Stochl, J., Upthegrove, R., Zammit, S., Wareham, N., Langenberg, C., ... Khandaker, G. M. (2021). Longitudinal trends in childhood insulin levels and body mass index and associations with risks of psychosis and depression in young adults. *JAMA Psychiatry*, 78, 416–425. <https://doi.org/10.1001/jamapsychiatry.2020.4180>
- Qiu, C., & Fratiglioni, L. (2015). A major role for cardiovascular burden in age-related cognitive decline. *Nature Reviews Cardiology*, 12(5), 267–277. <https://doi.org/10.1038/nrcardio.2014.223>
- R Core Team. (2012). A language and environment for statistical computing. Retrieved from <http://www.r-project.org/>
- Reiman, E. M., Chen, K., Caselli, R. J., Alexander, G. E., Bandy, D., Adamson, J. L., ... Papassotiropoulos, A. (2008). Cholesterol-related genetic risk scores are associated with hypometabolism in Alzheimer's-affected brain regions. *NeuroImage*, 40(3), 1214–1221. <https://doi.org/10.1016/j.neuroimage.2007.12.066>
- Reuter, M., & Fischl, B. (2011). Avoiding asymmetry-induced bias in longitudinal image processing. *NeuroImage*, 57(1), 19–21. <https://doi.org/10.1016/j.neuroimage.2011.02.076>
- Reuter, M., Rosas, H. D., & Fischl, B. (2010). Highly accurate inverse consistent registration: A robust approach. *NeuroImage*, 53(4), 1181–1196. <https://doi.org/10.1016/j.neuroimage.2010.07.020>
- Reuter, M., Schmansky, N. J., Rosas, H. D., & Fischl, B. (2012). Within-subject template estimation for unbiased longitudinal image analysis. *NeuroImage*, 61(4), 1402–1418. <https://doi.org/10.1016/j.neuroimage.2012.02.084>
- Richard, G., Kolskår, K., Sanders, A.-M., Kaufmann, T., Petersen, A., Doan, N. T., ... Westlye, L. T. (2018). Assessing distinct patterns of cognitive aging using tissue-specific brain age prediction based on diffusion tensor imaging and brain morphometry. *PeerJ*, 6, e5908. <https://doi.org/10.7717/peerj.5908>
- Richard, G., Kolskår, K., Ulrichsen, K. M., Kaufmann, T., Alnæs, D., Sanders, A.-M., ... Westlye, L. T. (2020). Brain age prediction in stroke patients: Highly reliable but limited sensitivity to cognitive performance and response to cognitive training. *NeuroImage: Clinical*, 25, 102159. <https://doi.org/10.1016/j.nicl.2019.102159>
- Ringen, P. A., Engh, J. A., Birkenaes, A. B., Dieset, I., & Andreassen, O. A. (2014). Increased mortality in schizophrenia due to cardiovascular disease—A non-systematic review of epidemiology, possible causes, and interventions. *Frontiers in Psychiatry*, 5, 137. <https://doi.org/10.3389/fpsy.2014.00137>
- Ringen, P. A., Faerden, A., Antonsen, B., Falk, R. S., Mamen, A., Rognli, E. B., ... Martinsen, E. W. (2018). Cardiometabolic risk factors, physical activity and psychiatric status in patients in long-term psychiatric inpatient departments. *Nordic Journal of Psychiatry*, 72(4), 296–302. <https://doi.org/10.1080/08039488.2018.1449012>
- Roalf, D. R., Quarmley, M., Elliott, M. A., Satterthwaite, T. D., Vandekar, S. N., Ruparel, K., ... Gur, R. E. (2016). The impact of quality assurance assessment on diffusion tensor imaging outcomes in a large-scale population-based cohort. *NeuroImage*, 125, 903–919. <https://doi.org/10.1016/j.neuroimage.2015.10.068>
- Røddevand, L., Steen, N. E., Elvsåshagen, T., Quintana, D. S., Reponen, E. J., Mørch, R. H., ... Andreassen, O. A. (2019). Cardiovascular risk remains

- high in schizophrenia with modest improvements in bipolar disorder during past decade. *Acta Psychiatrica Scandinavica*, 139(4), 348–360. <https://doi.org/10.1111/acps.13008>
- Ronan, L., Alexander-Bloch, A. F., Wagstyl, K., Farooqi, S., Brayne, C., Tyler, L. K., & Fletcher, P. C. (2016). Obesity associated with increased brain age from midlife. *Neurobiology of Aging*, 47, 63–70. <https://doi.org/10.1016/j.neurobiolaging.2016.07.010>
- Rueckert, D., Sonoda, L. I., Hayes, C., Hill, D. L. G., Leach, M. O., & Hawkes, D. J. (1999). Nonrigid registration using free-form deformations: Application to breast MR images. *IEEE Transactions on Medical Imaging*, 18(8), 712–721. <https://doi.org/10.1109/42.796284>
- Ruttman, E., Brant, L. J., Concin, H., Diem, G., Rapp, K., Ulmer, H., & the Vorarlberg Health Monitoring and Promotion Program Study Group. (2005). γ -Glutamyltransferase as a risk factor for cardiovascular disease mortality: An epidemiological investigation in a cohort of 163 944 Austrian adults. *Circulation*, 112(14), 2130–2137. <https://doi.org/10.1161/CIRCULATIONAHA.105.552547>
- Sanders, A.-M., Richard, G., Kolskär, K., Ulrichsen, K. M., Kaufmann, T., Alnæs, D., Beck, D., Dørum, E. S., de Lange, A.-M. G., Nordvik, J. E., & Westlye, L. T. (2021). Linking objective measures of physical activity and capability with brain structure in healthy community dwelling older adults. *MedRxiv*, January 28, 2021.21250529. <https://doi.org/10.1101/2021.01.28.21250529>
- Schmitt, A., Maurus, I., Rossner, M. J., Röh, A., Lembeck, M., von Wilmsdorff, M., ... Falkai, P. (2018). Effects of aerobic exercise on metabolic syndrome, cardiorespiratory fitness, and symptoms in schizophrenia include decreased mortality. *Frontiers in Psychiatry*, 9, 690. <https://doi.org/10.3389/fpsy.2018.00690>
- Shafiq, M. A., Dixon, M., Taylor, J. R., Rowe, J. B., Cusack, R., Calder, A. J., ... Matthews, F. E. (2014). The Cambridge Centre for Ageing and Neuroscience (Cam-CAN) study protocol: A cross-sectional, lifespan, multidisciplinary examination of healthy cognitive ageing. *BMC Neurology*, 14(1), 204. <https://doi.org/10.1186/s12883-014-0204-1>
- Smith, S. M. (2002). Fast robust automated brain extraction. *Human Brain Mapping*, 17(3), 143–155. <https://doi.org/10.1002/hbm.10062>
- Smith, S. M., Elliott, L. T., Alfaro-Almagro, F., McCarthy, P., Nichols, T. E., Douaud, G., & Miller, K. L. (2020). Brain aging comprises many modes of structural and functional change with distinct genetic and biophysical associations. *eLife*, 9, e52677. <https://doi.org/10.7554/eLife.52677>
- Smith, S. M., Jenkinson, M., Johansen-Berg, H., Rueckert, D., Nichols, T. E., Mackay, C. E., ... Behrens, T. E. J. (2006). Tract-based spatial statistics: Voxelwise analysis of multi-subject diffusion data. *NeuroImage*, 31(4), 1487–1505. <https://doi.org/10.1016/j.neuroimage.2006.02.024>
- Smith, S. M., Jenkinson, M., Woolrich, M. W., Beckmann, C. F., Behrens, T. E. J., Johansen-Berg, H., ... Matthews, P. M. (2004). Advances in functional and structural MR image analysis and implementation as FSL. *NeuroImage*, 23, S208–S219. <https://doi.org/10.1016/j.neuroimage.2004.07.051>
- Smith, S. M., Vidaurre, D., Alfaro-Almagro, F., Nichols, T. E., & Miller, K. L. (2019). Estimation of brain age delta from brain imaging. *NeuroImage*, 200, 528–539. <https://doi.org/10.1016/j.neuroimage.2019.06.017>
- Sone, D., Beheshti, I., Maikusa, N., Ota, M., Kimura, Y., Sato, N., ... Matsuda, H. (2019). Neuroimaging-based brain-age prediction in diverse forms of epilepsy: A signature of psychosis and beyond. *Molecular Psychiatry*, 26, 825–834. <https://doi.org/10.1038/s41380-019-0446-9>
- Spangaro, M., Mazza, E., Poletti, S., Cavallaro, R., & Benedetti, F. (2018). Obesity influences white matter integrity in schizophrenia. *Psychoneuroendocrinology*, 97, 135–142. <https://doi.org/10.1016/j.psychneuen.2018.07.017>
- Stan Development Team (2020). RStan: the R interface to Stan. R package version 2.21.2. Retrieved from <http://mc-stan.org/>
- Steffener, J. (2016). Differences between chronological and brain age are related to education and self-reported physical activity. *Neurobiology of Aging*, 40, 138–144.
- Taylor, J. R., Williams, N., Cusack, R., Auer, T., Shafto, M. A., Dixon, M., ... Henson, R. N. (2017). The Cambridge Centre for Ageing and Neuroscience (Cam-CAN) data repository: Structural and functional MRI, MEG, and cognitive data from a cross-sectional adult lifespan sample. *NeuroImage*, 144, 262–269. <https://doi.org/10.1016/j.neuroimage.2015.09.018>
- Tønnesen, S., Kaufmann, T., de Lange, A.-M. G., Richard, G., Doan, N. T., Alnæs, D., ... Selgren, C. (2020). Brain age prediction reveals aberrant brain white matter in schizophrenia and bipolar disorder: A multi-sample diffusion tensor imaging study. *Biological Psychiatry: Cognitive Neuroscience and Neuroimaging*, 5, 1095–1103. <https://doi.org/10.1016/j.bpsc.2020.06.014>
- Tønnesen, S., Kaufmann, T., Doan, N. T., Alnæs, D., Córdova-Palamera, A., van der Meer, D., ... Westlye, L. T. (2018). White matter aberrations and age-related trajectories in patients with schizophrenia and bipolar disorder revealed by diffusion tensor imaging. *Scientific Reports*, 8(1), 14129. <https://doi.org/10.1038/s41598-018-32355-9>
- Treder, M. S., Shock, J. P., Stein, D. J., du Plessis, S., Seedat, S., & Tsvetanov, K. A. (2021). Correlation constraints for regression models: Controlling bias in brain age prediction. *Frontiers in Psychiatry*, 12, 25. <https://doi.org/10.3389/fpsy.2021.615754>
- van Buuren, S., & Groothuis-Oudshoorn, K. (2011). mice: Multivariate imputation by chained equations in R. *Journal of Statistical Software*, 45, 1–67.
- Varatharajah, Y., Baradwaj, S., Kiraly, A., Ardila, D., Iyer, R., Shetty, S., & Kohlhoff, K. (2018). Predicting brain age using structural neuroimaging and deep learning. *BioRxiv*, 497925. <https://doi.org/10.1101/497925>
- Veraart, J., Fieremans, E., & Novikov, D. S. (2016). Diffusion MRI noise mapping using random matrix theory. *Magnetic Resonance in Medicine*, 76(5), 1582–1593. <https://doi.org/10.1002/mrm.26059>
- Verhaaren, B. F. J., Vernooij, M. W., de Boer, R., Hofman, A., Niessen, W. J., van der Lugt, A., & Ikram, M. A. (2013). High blood pressure and cerebral white matter lesion progression in the general population. *Hypertension*, 61(6), 1354–1359. <https://doi.org/10.1161/HYPERTENSIONAHA.111.00430>
- Vintimilla, R. M., Large, S. E., Gamboa, A., Rohlfing, G. D., O'Jile, J. R., Hall, J. R., ... Johnson, L. A. (2018). The link between potassium and mild cognitive impairment in Mexican-Americans. *Dementia and Geriatric Cognitive Disorders Extra*, 8(1), 151–157. <https://doi.org/10.1159/000488483>
- Wagenmakers, E.-J., Lodewyckx, T., Kuriyal, H., & Grasman, R. (2010). Bayesian hypothesis testing for psychologists: A tutorial on the Savage–Dickey method. *Cognitive Psychology*, 60(3), 158–189. <https://doi.org/10.1016/j.cogpsych.2009.12.001>
- Walhovd, K. B., Storsve, A. B., Westlye, L. T., Drevon, C. A., & Fjell, A. M. (2014). Blood markers of fatty acids and vitamin D, cardiovascular measures, body mass index, and physical activity relate to longitudinal cortical thinning in normal aging. *Neurobiology of Aging*, 35(5), 1055–1064. <https://doi.org/10.1016/j.neurobiolaging.2013.11.011>
- Wang, H.-T., Smallwood, J., Mourao-Miranda, J., Xia, C. H., Satterthwaite, T. D., Bassett, D. S., & Bzdok, D. (2020). Finding the needle in a high-dimensional haystack: Canonical correlation analysis for neuroscientists. *NeuroImage*, 216, 116745. <https://doi.org/10.1016/j.neuroimage.2020.116745>
- Weinstein, G., Maillard, P., Himali, J. J., Beiser, A. S., Au, R., Wolf, P. A., ... DeCarli, C. (2015). Glucose indices are associated with cognitive and structural brain measures in young adults. *Neurology*, 84(23), 2329–2337. <https://doi.org/10.1212/WNL.0000000000001655>
- Wersching, H., Duning, T., Lohmann, H., Mohammadi, S., Stehling, C., Fobker, M., ... Knecht, S. (2010). Serum C-reactive protein is linked to cerebral microstructural integrity and cognitive function. *Neurology*, 74(13), 1022–1029. <https://doi.org/10.1212/WNL.0b013e3181d7b45b>

- Williams, O. A., An, Y., Beason-Held, L., Huo, Y., Ferrucci, L., Landman, B. A., & Resnick, S. M. (2018). Vascular burden and APOE $\epsilon 4$ are associated with white matter microstructural decline in cognitively normal older adults. *NeuroImage*, 188, 572–583. <https://doi.org/10.1016/j.neuroimage.2018.12.009>
- Williams, V. J., Leritz, E. C., Shepel, J., McGlinchey, R. E., Milberg, W. P., Rudolph, J. L., ... Salat, D. H. (2013). Interindividual variation in serum cholesterol is associated with regional white matter tissue integrity in older adults. *Human Brain Mapping*, 34(8), 1826–1841. <https://doi.org/10.1002/hbm.22030>
- Williamson, W., Lewandowski, A. J., Forkert, N. D., Griffanti, L., Okell, T. W., Betts, J., ... Leeson, P. (2018). Association of Cardiovascular risk factors with MRI indices of cerebrovascular structure and function and white matter hyperintensities in young adults. *JAMA*, 320(7), 665–673. <https://doi.org/10.1001/jama.2018.11498>
- Wu, T.-H., Fann Jean, C.-Y., Chen Sam, L.-S., Yen Amy, M.-F., Wen, C.-J., Lu, Y.-R., ... Liou, H.-H. (2018). Gradient relationship between increased mean corpuscular volume and mortality associated with cerebral ischemic stroke and ischemic heart disease: A longitudinal study on 66,294 Taiwanese. *Scientific Reports*, 8. <http://dx.doi.org/10.1038/s41598-018-34403-w>
- Yamada, S., Tsuruya, K., Taniguchi, M., Tokumoto, M., Fujisaki, K., Hirakata, H., ... Kitazono, T. (2016). Association Between Serum Phosphate Levels and Stroke Risk in Patients Undergoing Hemodialysis: The Q-Cohort Study. *Stroke*, 47(9), 2189–2196. <https://doi.org/10.1161/STROKEAHA.116.013195>
- Yusuf, S., Hawken, S., & Ounpuu, S. (2004). Effect of potentially modifiable risk factors associated with myocardial infarction in 52 countries (the INTERHEART study): Case-control study. *ACC Current Journal Review*, 13(12), 15–16. <http://doi.org/10.1016/j.accreview.2004.11.072>

SUPPORTING INFORMATION

Additional supporting information may be found in the online version of the article at the publisher's website.

How to cite this article: Beck, D., de Lange, A.-M. G., Pedersen, M. L., Alnæs, D., Maximov, I. I., Voldsbekk, I., Richard, G., Sanders, A.-M., Ulrichsen, K. M., Dørum, E. S., Kolskår, K. K., Høgestøl, E. A., Steen, N. E., Djurovic, S., Andreassen, O. A., Nordvik, J. E., Kaufmann, T., & Westlye, L. T. (2021). Cardiometabolic risk factors associated with brain age and accelerate brain ageing. *Human Brain Mapping*, 1–21. <https://doi.org/10.1002/hbm.25680>